CHAPTER
1

Introduction

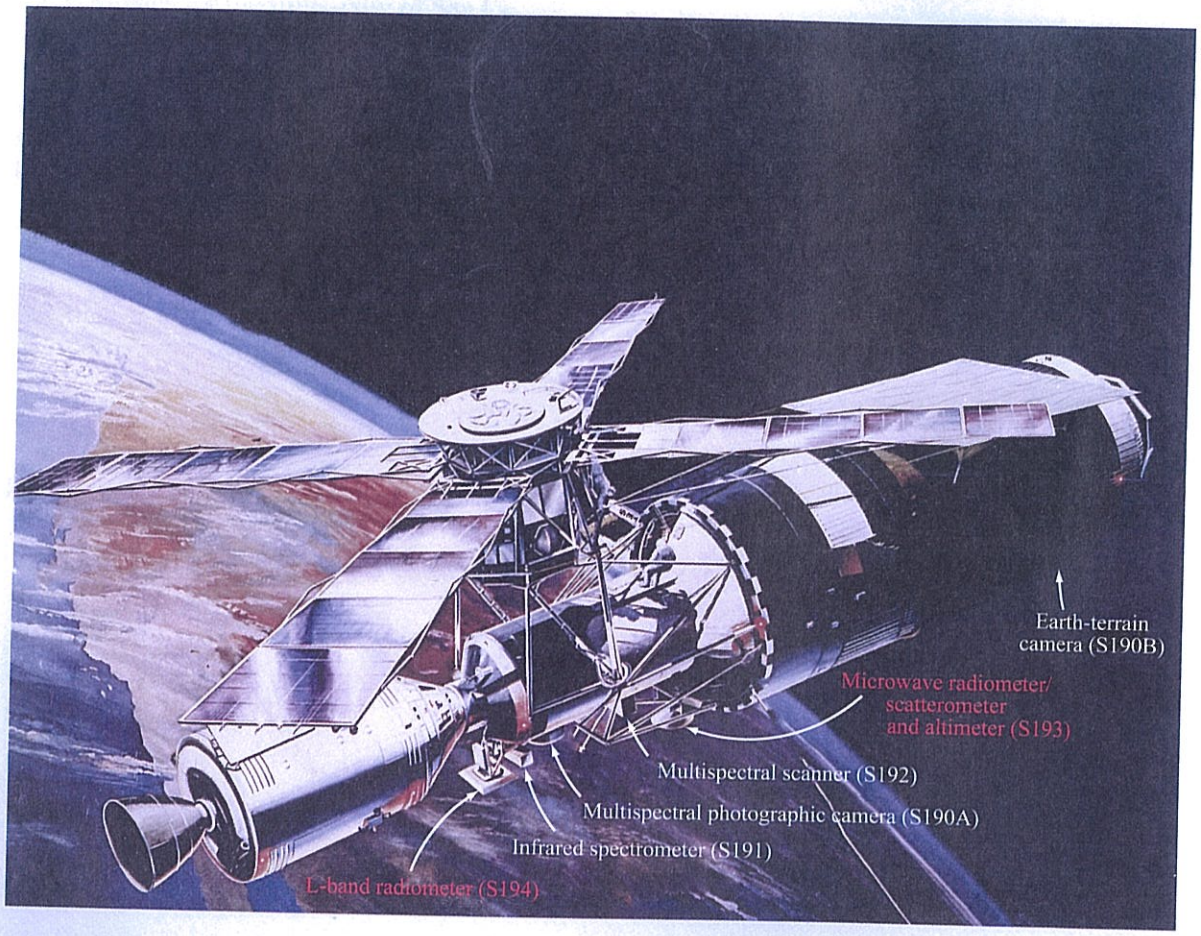

Skylab

CONTENTS

1-1 Why Microwaves for Remote Sensing?

Compared with aerial photography, which has been in use since the late 1800s, microwave remote sensing is relatively new, having been used in civilian applications only since the early 1960s. Given the success of photography, why use microwaves for remote sensing?

► Microwaves provide a different and unique view that offers new information about Earth's environment that often can be obtained in no other way. ◄

Microwaves can penetrate clouds—and to some extent rain—and do not rely on the sun as the source for illumination. These attributes allow sensing of the Earth independently of the time of day and under almost all weather conditions. Figure 1-1 illustrates the attenuating effect of clouds on radio transmission between space and the Earth surface as a function of electromagnetic wavelength. Clouds that are dense enough to completely obscure the ground, and thus preclude aerial or satellite optical imaging, have little effect on microwaves. Ice clouds have almost no effect at any wavelength longer than 1 cm, while water clouds have a significant effect only for wavelengths less than 2 cm. Rain has a greater effect than clouds, but as shown in Fig. 1-2, it is important only for wavelengths less than 4 cm. Active (radar) microwave sensors are thus able to observe the Earth's surface under almost all conditions.

► For passive microwave remote sensing (*radiometry*) the attenuation effects of clouds and rain can obscure the surface at some frequencies. However, this same attenuation provides an observable signal that can be exploited by microwave radiometers to gather information about key geophysical parameters of interest such as total liquid water fraction, cloud droplet size distribution, atmospheric temperature, and rain intensity. ◄

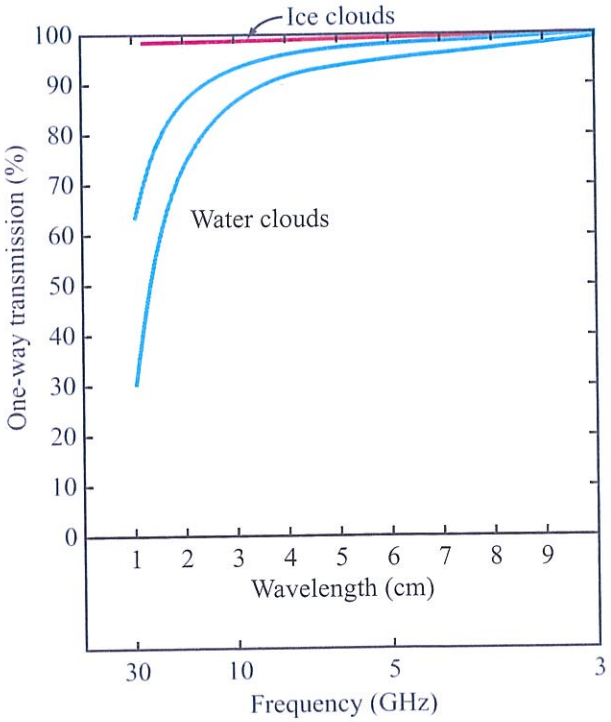

Figure 1-1: Attenuating effects of clouds on radio transmission from space to ground.

At longer wavelengths, radiometers are able to observe the surface—particularly in the polar regions—through clouds, whereas mapping such areas in the visible spectrum is much more difficult.

► Another reason for the use of microwaves is that they are able to penetrate more deeply into vegetation than optical waves can. ◄

A pictorial illustration of the relation between penetration depth and wavelength is shown in Fig. 1-3. The extent of penetration into vegetation depends upon the moisture content and density of the vegetation canopy, as well as upon the wavelength of the microwaves. Longer wavelengths penetrate much better than shorter wavelengths. Hence, shorter wavelengths yield information about the upper layers

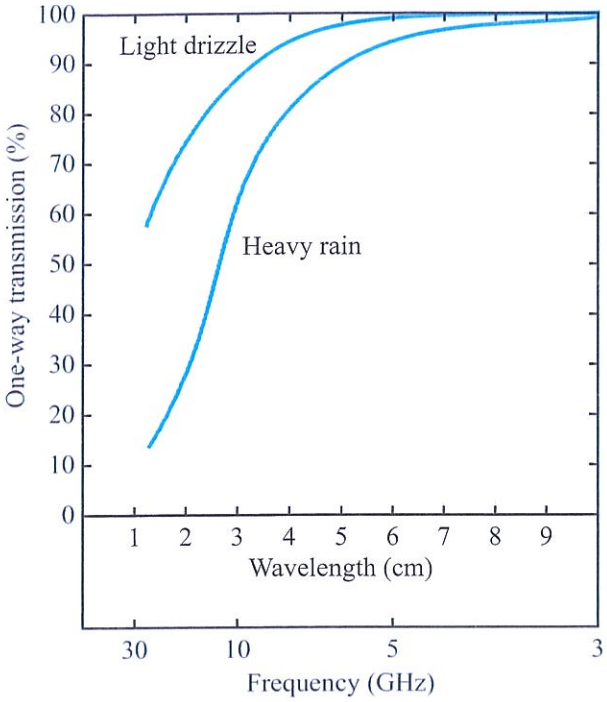

Figure 1-2: Attenuating effects of rain on radio transmission from space to ground.

of the vegetation, while longer wavelengths yield information about the lower layers and the ground beneath. Moreover, microwaves are able to penetrate significantly into the ground itself. Figure 1-4 illustrates the depth at which the microwave signal decreases by 63 percent for three different frequencies and three different types of soil. For dry soil the penetration depth at the lower microwave frequencies can be substantial, whereas penetration is limited for wet soil.

► A third, and perhaps the most important, reason for the use of microwaves is that the information available from microwaves is different from that available in the visible and infrared regions of the electromagnetic spectrum. ◄

In particular, microwave scattering from a natural surface is related to both the electrical (bulk-dieletric)

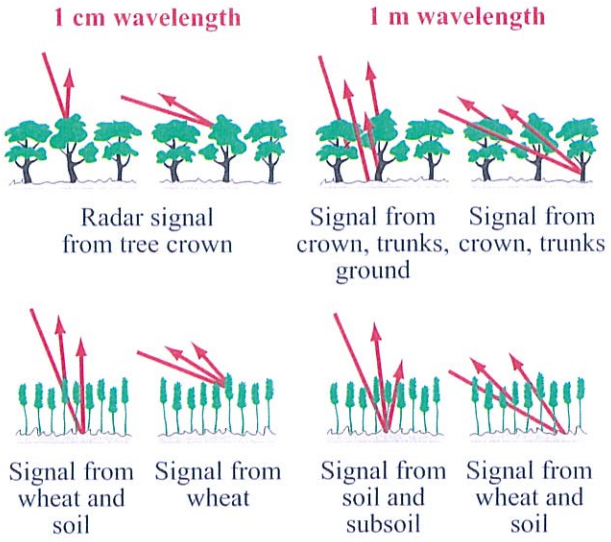

Figure 1-3: Illustration of radar signal penetration through and scattering by vegetation. There is more penetration if vegetation is dry than if wet.

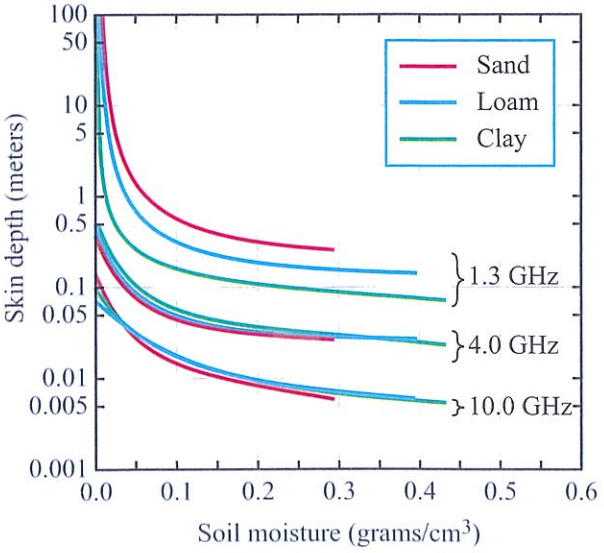

Figure 1-4: Skin depth as a function of soil volumetric water content, frequency, and soil type [from Ulaby et al., 1974].

and geometric (roughness) properties of the surface. With suitably designed sensors, it is thus possible to infer information about surface geometry as well as the electrical properties of the surface. Further, microwave-derived properties complement the information obtainable from visible and infrared radiation, facilitating studies of geometric, bulk-dielectric, and molecular-resonance properties of a surface feature.

1-2 A Brief Overview of Microwave Sensors

Microwave remote sensing instruments can be divided into two broad classes: ***passive***, known as ***radiometers***, and ***active***, known as ***radars*** (Fig. 1-5). Both include antennas and receivers, but radars differ from radiometers in that they include a transmitter as well. Both classes of sensors have been used on aircraft and spacecraft to study the Earth as well as other planets. These broad classes can be subdivided into subclasses based on their general operating characteristics and functions.

Active microwave sensors can be grouped into five general classes: ***synthetic-aperture radar*** (SAR) systems, ***side-looking airborne radar*** (SLAR), ***scatterometers***, ***altimeters***, and ***meteorological radars***. As suggested by the name, SAR employs synthetic-aperture antenna-processing techniques, whereas the other sensor systems typically use real-aperture antennas. ***Inverse synthetic-aperture radar*** (ISAR) is used for ground-based sensing of extra-terrestrial bodies.

► SAR and SLAR systems are designed to create images from moving platforms. ◄

Such systems operate by transmitting modulated pulses and using Doppler/range processing to construct backscatter images. SARs provide the highest resolution, but are significantly more complex than other sensors. Scatterometers measure radar backscatter very precisely, but they typically have lower resolutions than SARs. Altimeters are specialized radars designed to measure platform height, although other information can be extracted from the echo. Weather radars are specially designed scatterometers with ranging capability that measure rainfall and other meteorological phenomena. ***Interferometric SAR*** (InSAR or IFSAR) is a special SAR configuration used to measure topography and the motion of surfaces. Surveillance radars, which are designed for aircraft, ship, and missile detection and/or tracking, are treated in more detail in dedicated radar texts such as Richards et al. (2010) and Skolnik (1980).

► ***Radiometers*** are passive microwave sensors that observe thermal emission of microwave signals. ◄

The emission is related to the physical temperature and electrical properties of the sensed surface or volume, with modulation by the intervening atmosphere. Since they contain no transmitters, radiometers typically consume much less power. They frequently operate over a broader frequency range (bandwidth) than radar sensors and primarily rely on real-aperture antennas, although ***synthetic-aperture radiometers*** (interferometers) are also used for both Earth remote sensing and astronomical observation (Burke and Graham-Smith, 2002; Goodberlet, 2000; Le Vine, 1999; Ruf et al., 1988; Thompson et al., 1994; Wohlleben et al., 1991). ***Sounders*** are specialized radiometers designed for extracting vertical profiles of atmospheric parameters.

1-3 A Short History of Microwave Remote Sensing

1-3.1 Radar

The very first successful attempt at generating radio waves was conducted at a frequency of 200 MHz, which, by today's frequency allocation nomenclature, is in the UHF band and very close to the lower edge of the microwave band (300 MHz to 300 GHz). In 1886, Heinrich Hertz experimentally tested Maxwell's electromagnetic theory with resonators and demonstrated that reflections from various metallic and nonmetallic objects can indeed be detected.

Radar was first used to detect ships in 1903 by Hülsmeyer, who obtained a patent for his idea in 1904

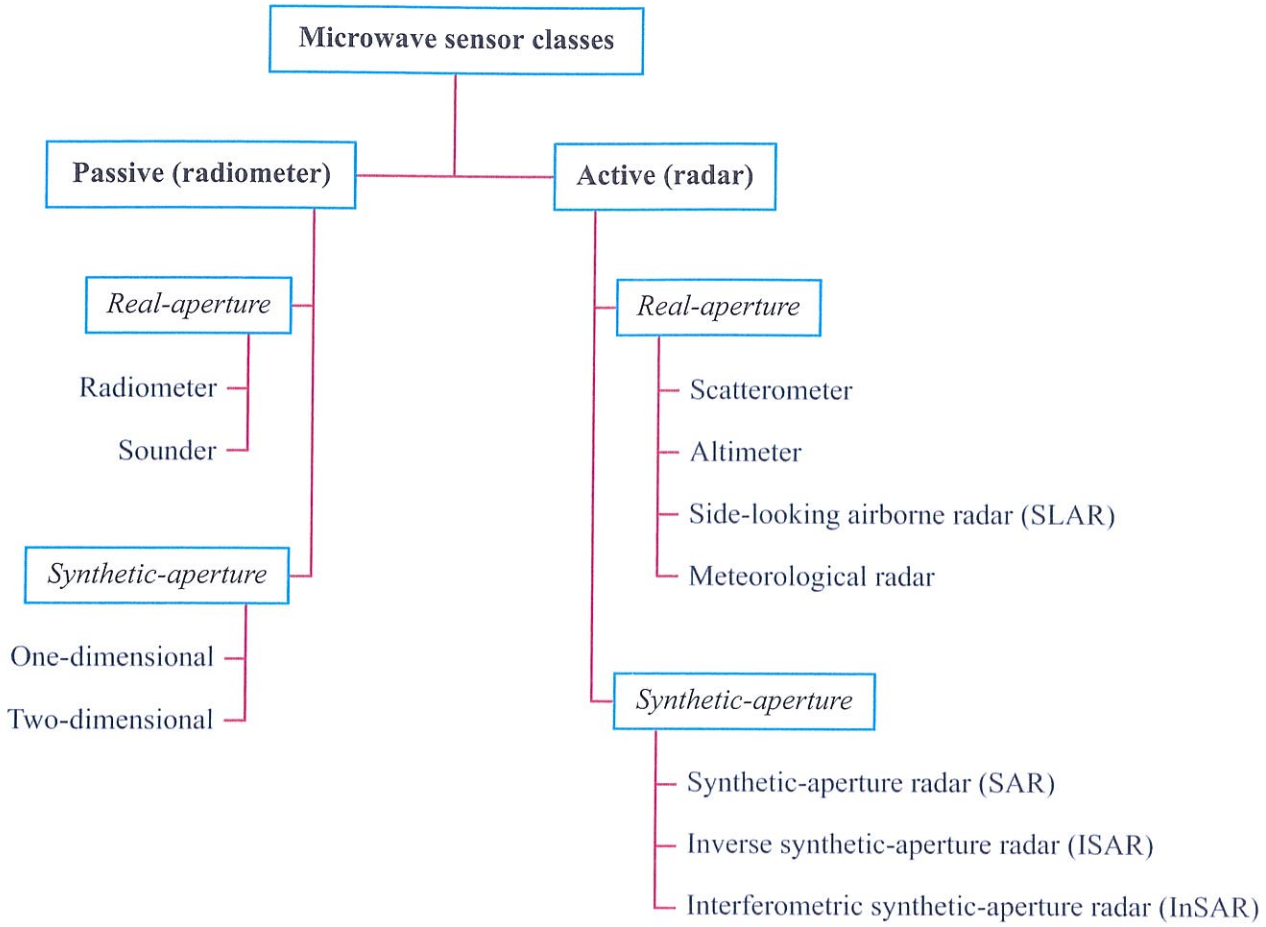

Figure 1-5: Major classes of microwave remote sensors.

(Hülsmeyer, 1904). Marconi (1922) predicted the use of radio for detection, but did not develop it. A. H. Taylor and others at the U.S. Naval Research Laboratory were pioneers in the development of radar as a tool for detecting ships and aircraft. The first experiment was conducted with a continuous-wave system in 1922 (Skolnik, 1980).

Interestingly, the first ***pulsed radar*** was used for remote sensing experiments in ionospheric sounding in 1925 (Breit and Tuve, 1926). Taylor, Breit, and Tuve transmitted pulses from a radio station and then observed the pulses that were reflected by the ionosphere at a separate location a few miles distant so as to measure the height of the ionosphere. The development of pulse radars for detecting objects closer to the Earth did not begin until the early 1930s (Taylor et al., 1934) and the first successful pulsed radar at the U.S. Naval Research Laboratory (NRL) operated in 1936. About this same time, pulse radars were developed in Great Britain under Sir Robert Watson-Watt (1957). The first ***airborne radars*** to be used extensively prior to World War II were frequency-modulated ***altimeters*** operating at about 400 MHz (Matsuo, 1938).

By the time of World War II, all the major participants had pulse-radar systems developed for the purpose of locating aircraft and/or ships. The

airborne radars deployed during the early part of World War II operated at long wavelengths (Rowe, 1948). Shortly thereafter, the MIT Radiation Laboratory (MIT Rad. Lab., 1948–52) in the United States and comparable laboratories in other countries demonstrated airborne radars operating at microwave frequencies that were capable of producing images of the ground. By 1946, radars producing images of the ground were in extensive use in the 3, 10, and 24 GHz bands. Other types of radar systems also were developed and widely used during World War II, including altimeters and radar *proximity fuses*. Proximity fuses permitted the detonation of artillery shells in the immediate vicinity of an aircraft in flight, thus damaging it without the necessity of a direct hit by a shell. It also permitted the bursting of shells well above the ground, thereby dispersing their destructive effect so that, again, a direct hit was not required.

Early airborne imaging radars required rotating antennas to scan the surface. The antennas were limited in size and thus restricted the image resolution. In the 1950s, a new type of radar, the side-looking airborne radar (SLAR), was developed. With the SLAR, finer-resolution images could be achieved because the antenna could be quite long since it was fixed parallel to the fuselage of the aircraft.

► SLAR scanning was achieved by a fixed beam pointed to the side, with the aircraft's motion moving the beam across the land, hence producing a scanned image. Images were recorded on long strips of film. ◄

Through the 1950s many different SLAR systems were developed, including systems that operated at 10 GHz (3 cm wavelength), 16 GHz (1.9 cm wavelength) and 35 GHz (8.6 mm wavelength). With these high frequencies and with antennas that were as long as 15 m, very fine-resolution images could be produced, extending to quite long ranges. By 1960, extensive imagery had been produced, but were unavailable on an unclassified basis; however, in 1964, images produced by the 8.6 mm AN / APQ-97 system were declassified. This data set clearly demonstrated the power of radar imaging as a tool for Earth observation and led to further development of imaging radars.

► In 1952, Wiley developed an airborne radar based on what he called a "Doppler beam-sharpening" system. This was the first of what is now known as synthetic-aperture radar (SAR). ◄

Wiley's first system operated at 75 MHz and looked to the side of the aircraft with a beam pointed about 45° ahead (this is now called "squint mode") (Cutrona, 1970). An independent development of a Doppler-processing radar was started in 1954 at the University of Illinois (Sherwin et al., 1962), where it was termed "synthetic-aperture." This work was transferred to the University of Michigan in 1956 (Cutrona et al., 1961). During the late 1950s and early 1960s, classified development of synthetic-aperture radar systems took place at the University of Michigan and at various companies. The first unclassified papers describing this new type of imaging radar appeared in 1961 (Cutrona et al., 1961, 1962). At the same time, similar developments were proceeding in other countries, including the USSR (Reutov and Mikhaylov, 1970), France, and the United Kingdom. However, papers in the open literature reporting these developments did not appear until after the 1961 papers in the U.S.

► A synthetic-aperture radar permitted the production of side-looking radar images whose pixel dimension in the along-track direction was independent of distance from the radar and could be much smaller than was possible for a SLAR with a feasibly short antenna. ◄

This represented a major step forward in improved resolution for airborne radars and made feasible the concept of fine-resolution spaceborne imaging radar. SAR and SLAR are discussed in Chapters 13 and 14.

The first scientific applications of imaging radar were to geological studies, but it was recognized from the beginning that many other land-use, water-resource, and vegetation studies were possible with imaging radars.

The first major radar mapping project was conducted by the U.S. Army and the Government of Panama in Oriente Province, Panama, in 1967 (Viksne et al., 1969). During the 1970s multiple-polarization research synthetic-aperture systems at 1.25 GHz and about 9 GHz were flown by the Environmental Research Institute of Michigan (ERIM) (Rawson and Smith, 1974) and the Jet Propulsion Laboratory (JPL) (Schaber et al., 1980). The production of multiple-polarization, multiple-frequency images has contributed significantly to the knowledge of the capabilities of imaging radar in remote sensing. This then led to fully-polarimetric imaging radars (Ulaby and Elachi, 1990; Cloude and Pottier, 1996; Touzi et al., 2004). The development of interferometric SAR systems has enabled the generation of global topography maps from space (Farr et al., 2007; Hanssen, 2001; Zebker and Goldstein, 1986). Technology for building airborne SARs has continued to evolve, resulting in the reduction of sensor size and improved imaging resolution. Spatial resolutions finer than 10 cm have been achieved (Doerry et al., 2005).

The use of radar to observe weather conditions began with early ground-based radars whose operators noticed that the height of the "grass" (the reflection from ocean waves) was related to wind conditions. Experiments showed that rain, snow, and hail could be mapped with radar. In the U.S., the first weather radars were developed in the 1950s. The first civilian Doppler radar specifically deployed to study the morphology of storms was set up at the National Severe Storms Laboratory in Oklahoma in 1971 (Cobb, 2004). Other meteorological (weather) radars followed, which led to the deployment of the ***NEXRAD*** network of meteorological radars, which eventually achieved (essentially) complete coverage of the U.S. Other nations have deployed similar networks. These radars measure rain and wind at multiple heights, and provide storm warnings (Meischner, 2004). They are familiar to the general public from weather forecast broadcasts.

Spaceborne radars

Radars were first used in space for spacecraft docking, but have been extensively used for imaging, altimetry, and wind measurement. While spaceborne radars have been developed and flown by the military, we focus on civilian applications. Table 1-1 summarizes the history of imaging radars flown on civilian spacecraft. The first spaceborne imaging radars were used to study cloud-covered Venus and have been used to study the moon Titan (West et al., 2009). Beginning in the late 1970s the Soviet Union developed and flew a series of SLARs to observe Earth as part of its ***Okean missions***, which also included scanning radiometers. These early radars had very low resolution.

Proposals for spaceborne synthetic-aperture Earth-observation radars were made in the early 1960s, but the first such radar to fly in space was on the oceanographic satellite ***Seasat*** that was launched in June 1978; see Fig. 1-6 (Jordan, 1980). Operating for only three months, this system produced many millions of square kilometers of high-resolution radar imagery. Several shuttle SAR missions were flown through the 1980s, 1990s, and early 2000s, including the ***Shuttle Radar Topography Mission*** (SRTM), which used ***radar interferometry*** to measure global surface topography (Farr et al., 2007). Many other spaceborne SAR systems have been flown or are in various planning stages.

Two other classes of radars have been flown extensively on spacecraft: scatterometers and altimeters.

> ▶ A ***scatterometer*** (the term was coined in 1965 by R. K. Moore) is a device used for measuring the radar scattering coefficient quantitatively. ◀

Scattering-coefficient measurements were made during World War II (Kerr and Goldstein, 1951; Davies and MacFarlane, 1946) and continued thereafter (e.g., MacDonald, 1956; Rouse, 1969). A summary of many of the scattering measurements made prior to 1975 is provided by Long (1975).

The flight of the S-193 scatterometer onboard ***Skylab*** in 1974 was conducted to measure scattering from space. It demonstrated the ability of radar to infer near-surface wind speed from space (Moore and Young, 1977). The success of this experiment led to the flight of the scatterometer (SASS) on the Seasat oceanographic satellite launched in 1978 (Grantham et al., 1977). This multiantenna fan-beam Doppler scatterometer was the

Table 1-1: Overview of spaceborne SAR sensors and their main characteristics [Moreira et al., 2013].

Sensor	Operation	Frequency Band (Polarization)	Comments	Institution, Country
Seasat	1978	L (hh)	First civilian SAR satellite, operation for only ca. three months	NASA/JPL, USA
SIRA-A, SIR-B	1981, 1984	L (hh)	Shuttle radar missions	NASA/JPL, USA
ERS-1/2	1991–2000/ 1995–2011	C (vv)	European Remote Sensing Satellites (first European SAR satellites)	ESA, Europe
J-ERS-1	1992–1998	L (hh)	Japanese Earth Resource Satellite (first Japanese SAR satellite)	JAXA, Japan
SIR-C/X-SAR	April and October 1994	L & C (quad) X (vv)	Shuttle imaging radar mission, first demonstration of spaceborne multifrequency SAR	NASA/JPL, USA DLR, Germany ASI, Italy
Radarsat-1	1995–today	C (hh)	First Canadian SAR satellite, swath width of up to 500 km with Scan SAR imaging mode	CSA, Canada
SRTM	Feb. 2000	C (hh+vv) and X (vv)	Shuttle Radar Topography Mission, first spaceborne interferometric SAR	NASA/JPL, USA DLR, Germany ASI, Italy
ENVISAT/ASAR	2002–2012	C (dual)	First SAR satellite with Transmit/ Receive module technology, swath width up to 400 km	ESA, Europe
ALOS/PALSAR	2006–2011	L (quad)	Advanced Land Observing Satellite (Daichi), swath width up to 360 km	JAXA, Japan
TerraSAR-X/ TanDEM-X	2007–today 2010–today	X (quad)	First bi-static radar in space, resolution up to 1 m, global topography available by end of 2014	DLR/Astrium, Germany
Radarsat-2	2007–today	C (quad)	Resolution up to: 1 m ×3 m (azimuth × range), swath width up to 500 km	CSA, Canada
COSMO-SkyMed-1/4	2007 . . . 2010–today	X (dual)	Constellation of four satellites, up to 1 m resolution	ASI/MID, Italy
RISAT-1/2	2008–today	C (quad)	Follow-on satellite (RISAT-1a) to be launched in 2016, RISAT-3 (L-band) in development	ISRO, India
HJ-1C	2012–today	S (vv)	Constellation of four satellites, first satellite launched in 2012	CRESDA/CAST/ NRSCC, China
Kompsat-5	Launch scheduled in 2013	X (dual)	Korea Multi-Purpose Satellite 5, resolution up to 1 m	KARI, Korea
PAZ	Launch scheduled in 2013	X (quad)	Constellation with TerraSAR-X and TanDEM-X planned	CDTI, Spain
ALOS-2	Launch scheduled in 2013	L (quad)	Resolution up to: 1 m ×3 m (azimuth × range), swath width up to 490 km	JAXA, Japan
Sentinel-1a/1b	Launch scheduled in 2013/2015	C (dual)	Constellation of two satellites, swath width up to 400 km	ESA, Europe
Radarsat Constellation-1/2/3	Launch scheduled in 2017	C (dual)	Constellation of three satellites, swath width up to 500 km	CSA, Canada
SAOCOM-1/2	Launch scheduled in 2014/2015	L (quad)	Constellation of two satellites, fully polarimetric	CONAE, Argentina

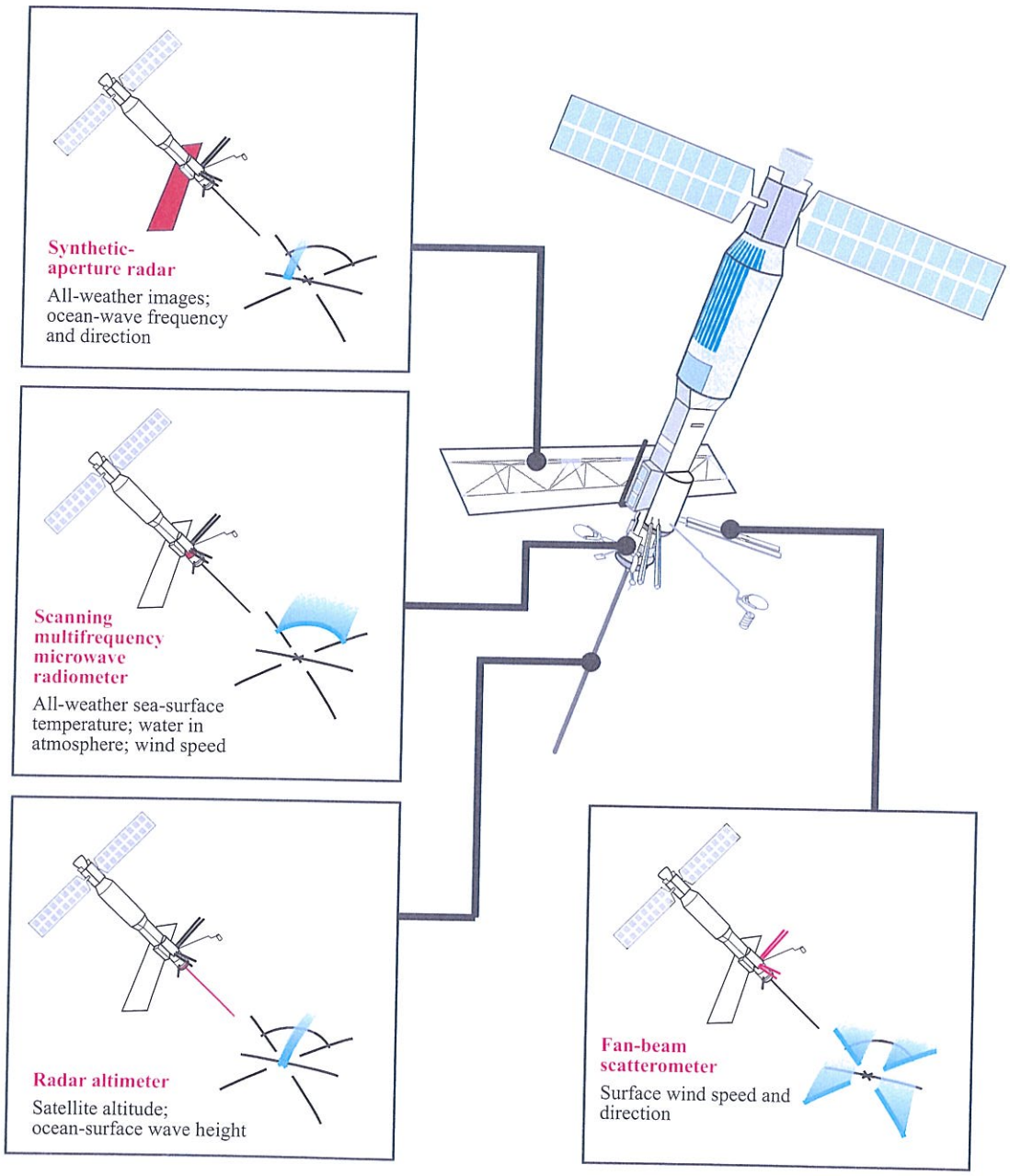

Figure 1-6: The Seasat-1 satellite, launched in 1978, with an illustration of the antenna illumination patterns for each of its microwave sensors.

Table 1-2: Operational scatterometers on spacecraft.

	SASS	ESCAT	NSCAT	SeaWinds	ASCAT	OSCAT
Frequency	14.6 GHz	5.3 GHz	13.995 GHz	13.6 GHz	5.3 GHz	13.6 GHz
Antenna azimuths	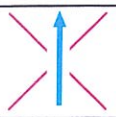		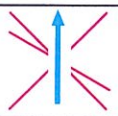			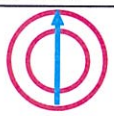
Polarizations	vv and hh	vv only	vv and hh	h-outer/h-inner	v only	v-outer/h-inner
Beam resolution	Fixed Doppler	Range gate	Variable Doppler	Pencil-beam	Range gate	Pencil-beam
Science modes	Many	SAR wind	Wind only	Wind/hi-res	Wind only	Wind/hi-res
Resolution (σ^0)	Normally 50 km	50 km	25 km	Egg: 25×35 km Slice: 6×25 km	25/50 km	Egg: 30×68 km Slice: 5×30 km
Swath, km	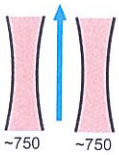	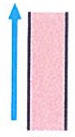	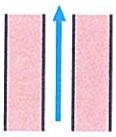	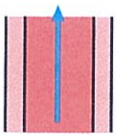	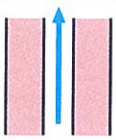	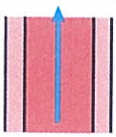
Incidence angles	0°–70°	18°–59°	17°–60°	46° & 54.4°	25°–65°	49° & 57°
Daily coverage	Variable	< 41%	78%	92%	65%	> 90%
Mission & dates	Seasat: 6/78–10/78	ERS-1: 92–96 ERS-2: 95–01	ADEOS-I: 8/96–6/97	QuikSCAT: 6/99-11/09 ADEOS II: 1/02–10/02	METOPD: 6/2007– METOPB: 9/2012–	OceanSat-2: 10/09–

first scatterometer designed for more than just research, and was operationally used for wind observation. It led a long series of operational scatterometer missions designed for wind observation (see Table 1-2). The Seasat scatterometer used four orthogonal fan beams [see Fig. 1-7(a)], to collect measurements at various incidence and azimuth angles of the same location on the surface, which enabled estimation of near-surface wind speed and direction. A number of follow-on instruments, such as the ***ERS-1/2*** scatterometer (1991-2011) (Attema, 1991), the ***NASA Scatterometer*** (NSCAT) (1996–1997) (Naderi et al., 1991), and the ***advanced scatterometer*** (ASCAT) (2008-present) (Figa-Saldaña et al., 2002), have used fan-beam antennas and employed either Doppler filters and/or range gating. The ***SeaWinds scatterometer*** (1999–2010 and 2006) (Spencer et al., 2000, 2003) was the first spaceborne wind scatterometer to use a dual-rotating beam. It was followed by the ***Indian Oceansat-2*** scatterometer (Parmar et al., 2006).

Wind scatterometers have become a standard instrument for satellite wind measurement. The scattering measurements from these sensors have been extensively used for other applications such as the mapping of sea-ice type and extent, detection of icebergs, and measuring soil moisture and vegetation density (Liu, 2002). A global view of the radar backscatter of the Earth's surface as observed by the SeaWinds scatterometer is shown in Fig. 1-8. Advanced capability scatterometers with higher resolution and dual-frequency have been proposed for the future (e.g., Long et al., 2009). The ***Soil Moisture Active Passive*** (SMAP) mission planned for launch in 2014–15 will employ a low-resolution L-band scatterometer/imager in conjunction with an L-band radiometer to improve the accuracy of soil moisture measurements (Entekhabi et al., 2010).

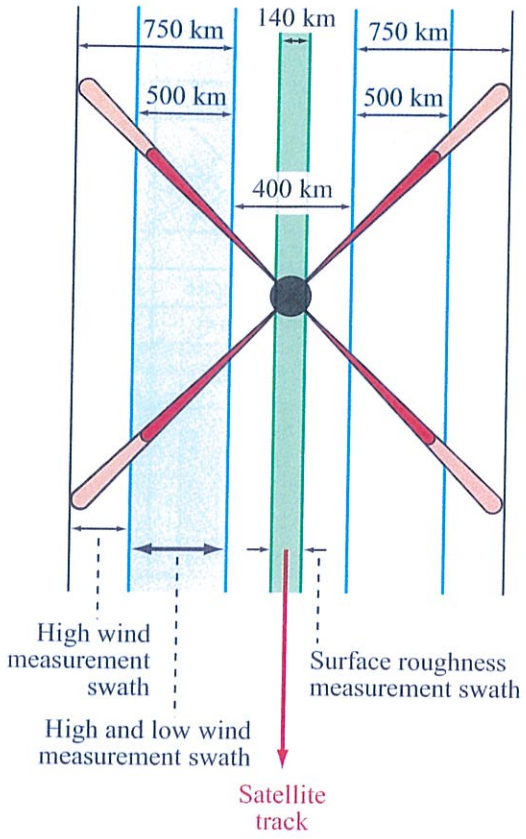

(a) Fan-beam antenna pattern (Seasat)

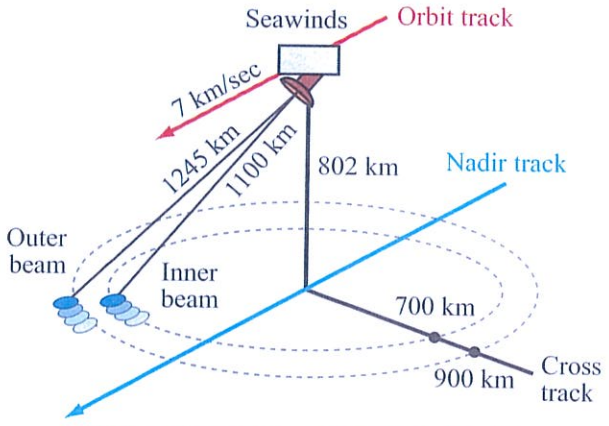

(b) Rotating antenna pattern (SeaWinds)

Figure 1-7: (a) Fan-beam antenna pattern for the Seasat scatterometer. (b) Rotating antenna pattern for the SeaWinds scatterometer. These are representative examples of the two major types of spaceborne scatterometers, fan-beam and scanning pencil-beam.

Satellite altimeters have been widely used for ocean studies and have become essential tools for the study of ocean circulation (Fu and Cazenave, 2001). Altimeters have also been used for measuring the topography of other planets such as perpetually cloud-covered Venus. Table 1-3 summarizes the history of satellite altimeters. Satellite altimeters provide very precise measurements of the distance from the satellite to the surface, and often include radiometers to enable correction for atmospheric delay. Coupled with precise orbit determination, very accurate surface topography can be derived. This information is useful for determining the geoid (the gravitational field of the Earth). Ocean topography measurements enable mapping of undersea topography and derivation of ocean currents. Wind speed can also be estimated. Figure 1-9 illustrates the derived shape of the geoid measured by the ***ERS-1 altimeter***. Planned developments in altimetry include a wide-swath system (Rodriguez and Pollard, 1999; Pollard et al., 2002). By examining the shape of the pulse return to a spaceborne radar altimeter over the sea, one also may establish the height of the waves beneath the spacecraft (Sandwell, 1991).

The ***Tropical Rain Mapping Mission*** (TRMM) ***Precipitation Radar*** is the first meteorological radar to be launched in space for mapping rain distributions. Launched in 1997 in an equatorial orbit and operating at Ku band, the TRMM PR used an electronically-scanned antenna to measure rainfall over a 50 km swath at a 4 to 5 km horizontal and 250 m vertical resolution (Kozu et al., 2001). The ***CloudSat*** satellite launched in 2006 carried a 94 GHz radar designed for vertically profiling clouds and precipitation along its nadir track (Tanelli et al., 2008).

1-3.2 Radiometers

► All matter radiates electromagnetic energy as a consequence of the movement of atoms and molecules in its material. ◄

A material also may absorb and/or reflect energy incident upon it. The spectral, polarization, and angular variations of the radiation emitted, absorbed, and

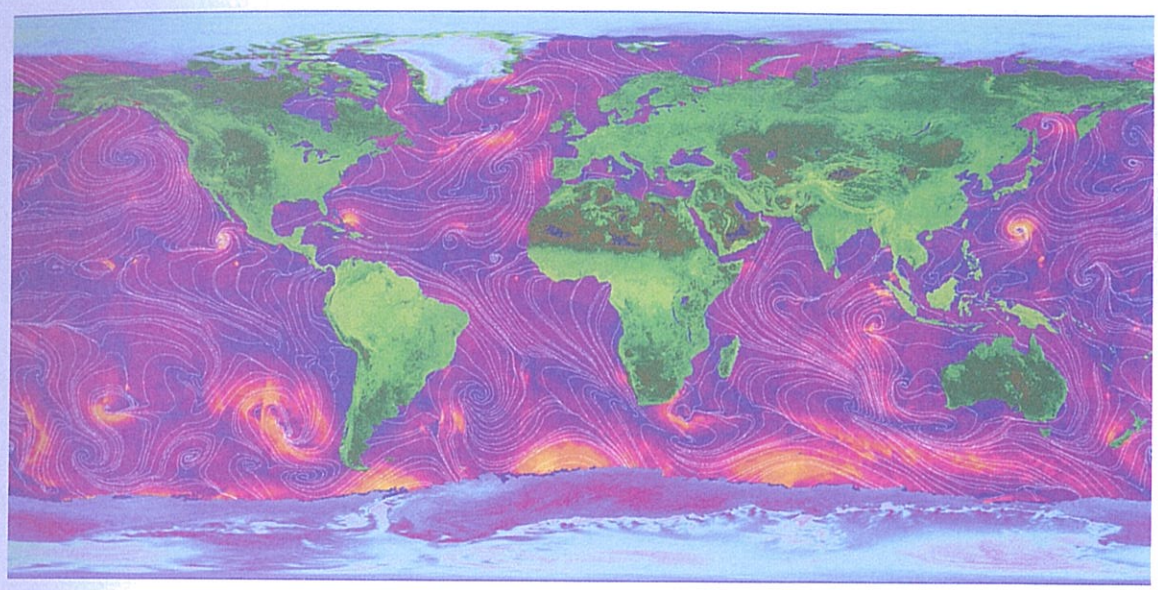

Figure 1-8: Global backscatter over land and ice derived from the SeaWinds spaceborne scatterometer. Wind speed and direction derived from ocean backscatter is shown over the ocean.

Table 1-3: History of civilian remote sensing altimeters on spacecraft.

Years	Spacecraft/Instrument	Band	Height accuracy[a] (cm)
1973	Skylab/S193	Ku	–
1975	Geos3	C	–
1978	Seasat/ALT[b]	Ku	10
1983	Venera 15/16[b]	S (8 cm)	
1985–1990	Geosat[d]	Ku	
1978–1992	Pioneer Venus-1/ORAD[b]	S (1.757 GHz)	
1990–1992	Magellan/ALT[b]	S (2.385 GHz)	3000
1991–1996	ERS-1/RA[d]	Ku	
1995–2011	ERS-2/RA[d]	Ku	
1981–2006	TOPEX-Poseidon/SSALT, NRA[d]	C, Ku	5
1997–	Cassini/ALT[b]	Ku	100
1998–2008	GFO[d]	C, Ku	
2001–	Jason-1/Poseidon-2[d]	C, Ku	
2002–2008	Envisat/RA-2[d]	Ku	
2006–	CloudSat/CPR[e]	W	5000
2008–	Jason-2/Poseidon-3[d]	C, Ku	2.5
2010–	Cryosat-2/Siral[c]	Ku	
2011–	HaiYang-2[d]	C, Ku	
2013	Saral/AltiK[d]a	Ka	

[a]Reported/estimated based on post processing; [b]Designed for planetary topography measurement; [c]Designed primarily for ice-sheet elevation and sea-ice freeboard; [d]Primarily designed for ocean topography; [e]Designed for cloud profiling.

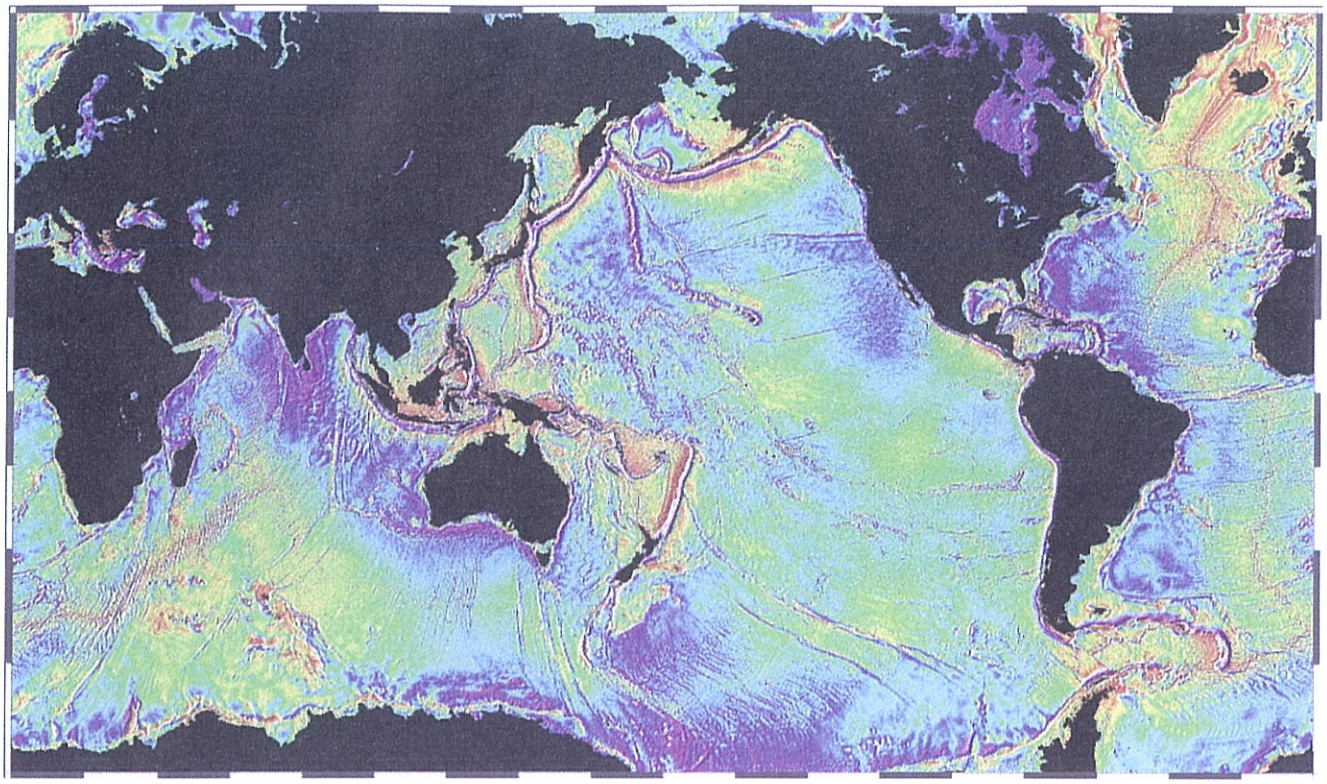

Figure 1-9: Shape of the geoid derived from spaceborne altimetry data by the ERS-1 altimeter. [Courtesy of D. Sandwell and W. Smith.]

scattered by a medium are governed by the geometrical configuration of the surface and interior of the medium, and by the spatial distributions of its temperature and dielectric properties. By measuring the electromagnetic energy radiated by a material, it is possible to infer some of these properties.

► Radiometry is the measurement of electromagnetic radiation. A ***microwave radiometer*** is a highly sensitive receiver capable of measuring low levels of microwave radiation. ◄

When a scene, such as terrain, is observed by a microwave radiometer (via its antenna beam), the radiation received by the antenna is partly due to self-emission by the scene and partly due to reflected radiation originating from the surroundings, such as the atmosphere. Through proper choice of the radiometer instrument parameters (wavelength, polarization, and viewing angle), it is sometimes possible to establish useful relations between the magnitude of the energy received by the radiometer and specific terrestrial or atmospheric parameters of interest. For example, observations of bare soil surfaces have shown that the radiometric response in the 20 to 30 cm wavelength range is influenced strongly by the soil moisture content (Schmugge, 1978). Such a dependence can be used over large areas to remotely map soil moisture content, an important physical parameter in many hydrological, agricultural, and meteorological applications. In many cases, multiwavelength observations can be processed to estimate more than one geophysical variable or to

predict the profile of a particular variable. Satellite-borne radiometer systems employ multiwavelength radiometric observations to generate global maps of atmospheric temperature profiles and of total water vapor and liquid water over the ocean.

Microwave radiometric techniques were first developed in the 1930s and 1940s to measure electromagnetic energy of extraterrestrial origin—antennas were pointed away from the Earth. Terrestrial microwave radiometric remote sensing had its beginnings in the late 1950s. Using a 4.3 mm wavelength radiometer, which had been developed to measure the solar temperature and atmospheric attenuation, Straiton's group at the University of Texas made radiometric observations of several terrestrial materials, such as water, wood, grass, and asphalt (Straiton et al., 1958). These observations represent the first deliberate effort in which the radiometer antenna was pointed "downward" rather than "upward."

Since then, the science of microwave radiometry has established itself as an integral part of the general field of environmental remote sensing. Numerous investigations have been conducted to evaluate the use of passive microwave sensors for meteorological, hydrological, oceanographic, and military applications. Experience with microwave radiometric data acquisition from spacecraft dates back to December 14, 1962, when the sensors aboard the ***Mariner 2*** spacecraft provided the first close observation of the planet Venus (Barrett and Lilley, 1963). Among the sensors flown aboard Mariner 2 was a two-channel microwave radiometer operating at wavelengths of 1.35 and 1.9 cm. Passive observations of the planet Earth were initiated in 1968 by the Russian satellite ***Cosmos 243***, which was equipped with four microwave radiometers (Basharinov et al., 1971). The 1978 Seasat-1 spacecraft included a microwave radiometer, as well as several different microwave radars, as shown in Fig. 1-6 (Barrick and Swift, 1980).

► Since 1968, microwave radiometers have been carried aboard many spacecraft (Table 1-4) and have become a standard tool for Earth observation, particularly over the ocean. ◄

Early radiometers had a limited number of channels, but recent radiometers have many channels, which may include fully polarimetric capability. Figure 1-10 illustrates global brightness temperature measurements of the Earth collected by the ***Advanced Microwave Scanning Radiometer*** (AMSR). The linear spatial resolution of these radiometer images is comparatively coarse, on the order of 25 to 50 km, which is typical of many spaceborne radiometers flown to date (Table 1-4). This is a consequence of the fact that the spatial resolution of a radiometer is governed by the antenna beamwidth and the platform altitude. Since the beamwidth is approximately equal to the reciprocal of the number of wavelengths across the antenna, very narrow beamwidths require very large antenna sizes. This problem is particularly acute for low frequency radiometer systems, which are desirable for measuring sea surface salinity and soil moisture. To overcome this limitation, ***synthetic-aperture radiometer systems***, also known as ***interferometers***, have been developed to improve radiometric imaging resolution. Interferometers were originally developed for use in radio astronomy (Ryle, 1952; Ryle and Hewish, 1960).

Airborne synthetic-aperture radiometers were operated as early as 1990 (Le Vine, 1999). The first synthetic-aperture radiometer to fly in space was the ***Soil Moisture and Ocean Salinity*** (SMOS) mission launched in 2009. Using 69 antennas arrayed along three

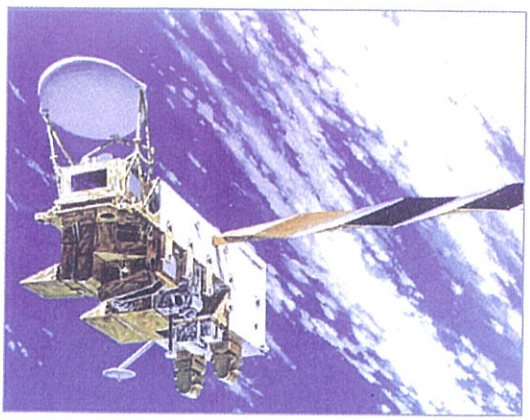

AMSR

Table 1-4: History of microwave radiometry on spacecraft.

Year(s)	Spacecraft Instrument Acronym	Frequencies (GHz)	Antenna type	Swath width (km)	Resolution[b] (km)
1962	Mariner 2 Venus Flyby	15.8, 22.4	mechanically scanned parabola	planetary	1300[a]
1968	Cosmos 243	3.5, 8.8, 22.3, 37	horns		13
1972	Nimbus 5 / ESMR	19.3	electrically scanned array	3000	25
	Nimbus 5 / NEMS	22.2, 31.4, 53.6, 54.9, 58.8	lens-loaded horns	nadir	200
1973	Skylab / S193	13.9	mechanically scanned parabola	180	16
	Skylab / S194	1.4	phased-array	nadir	115
1974	Meteor	37			
1975	Nimbus 6 / ESMR	19.3	electrically scanned array	3000	20 × 43
	Nimbus 6 / SCAMS	22.2, 31.6, 52.8, 53.8, 55.4	rotating hyperbolic mirrors	2700	150
1978	DMSP / SSM/T	50.5, 54.2, 54.3, 54.9, 58.4, 58.8, 59.4	rotating mirror	1600	175
1978, '78	TIRO N/MSU	50.3, 53.7, 55.09, 57.6	rotating mirror	2300	110
1978–87	Seasat 1 / SMMR	6.6. 10.7, 18, 21, 37	oscillating offset parabolic reflector	600	14 × 21
1978–	Nimbus 7 /SMMR	6.6. 10.7, 18, 21, 37	oscillating offset parabolic reflector	800	18 × 27
1987, '90, '91 '97, '99	DMSP /SSM/I	19.35, 22.2, 37, 85.5	spinning offset parabolic reflector	1400	15 × 13
1989	COBE	31.56, 53, 90	differential horns	full-sky	
1997–	TRMM TMI	10.7, 19.3, 21.3, 37, 85.5	spinning offset parabolic reflector	878	6
1998, '00, '02, '05	DMSP / AMSU-A/B	23.8, 89, 31.4	spinning offset reflector	1650	45
2001–11	Aqua / AMSR-E	6.9, 10.7, 18.7, 23.8, 36.5, 89	spinning offset parabolic reflector	1445	4 × 6
2001	WMAP	22, 30, 40, 60, 90	differential horns	full-sky	
2002	ADEOS-II / AMSR	6.9, 10.7, 18.7, 23.8, 36.5, 89	spinning offset parabolic reflector	1400	4 × 6
2003–	Coriolis / WindSat	6.68, 10.7, 18.7, 23.8, 37.0	spinning offset parabolic reflector	1000/400 (fore/aft)	8 × 13
2009	SMOS	1.41	synthetic aperture	1500	40
2011	Aquarius	1.413	pushbroom offset parabolic reflector	340	62 × 68
2014–15	SMAP	1.41	conically scanning mesh reflector	1000	39 × 47

[a]Courtesy of L. King, NASA/GSFC; [b]resolution of highest frequency

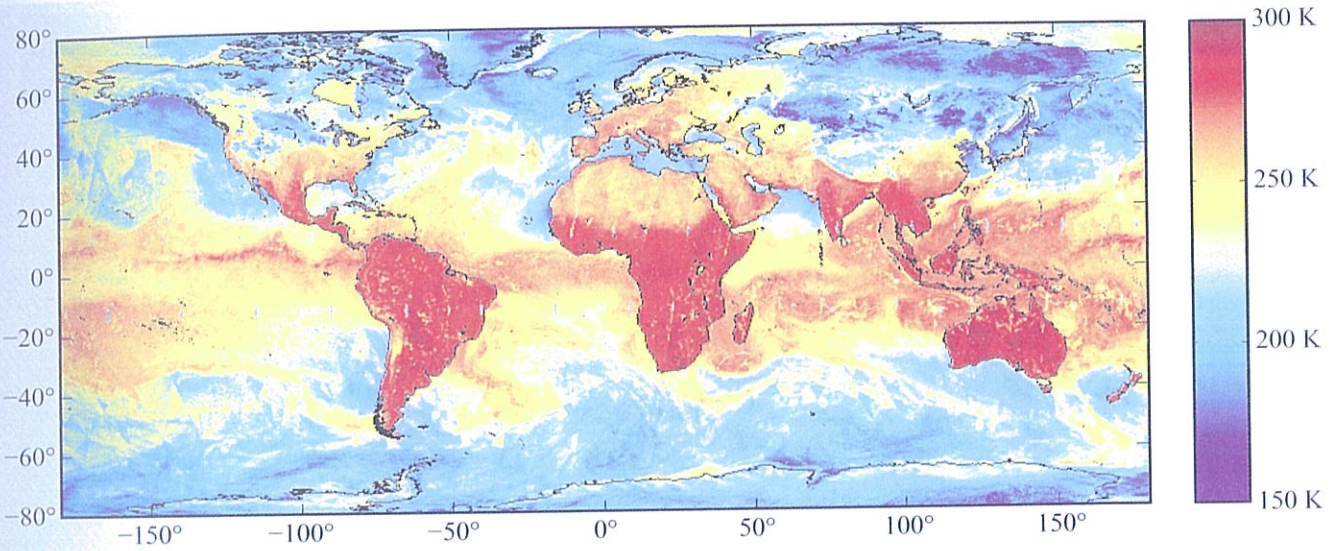

(a) AMSR-E, 89.0 GHz h-polarized

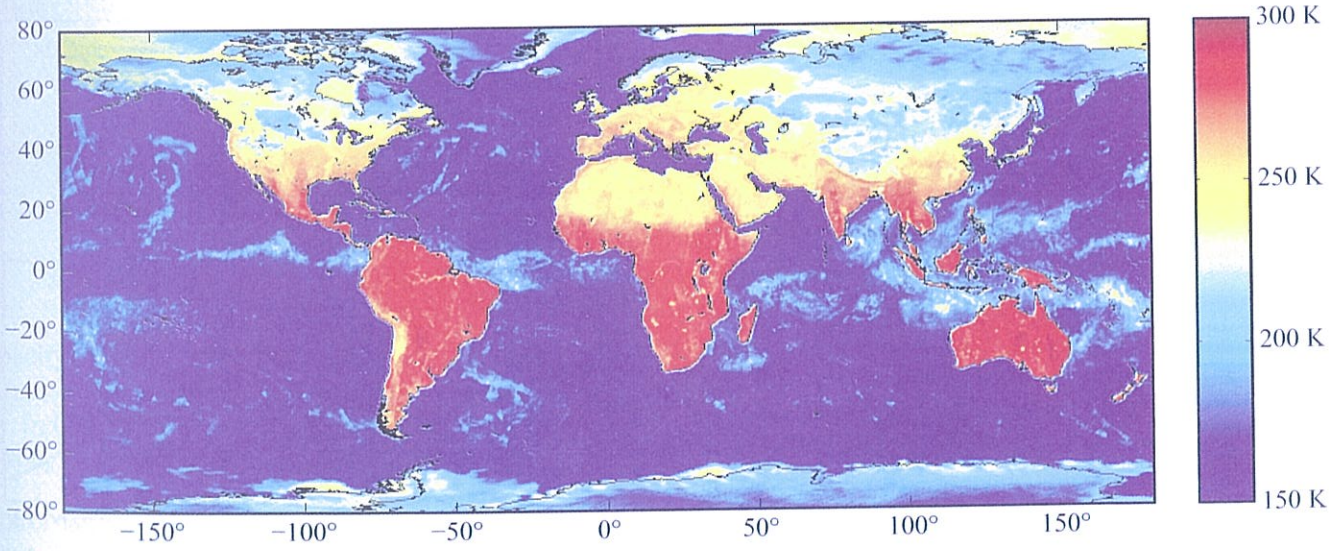

(b) AMSR-E, 36.5 GHz h-polarized

Figure 1-10: Passive microwave images of the measured brightness temperature of the globe collected by the Advanced Microwave Sensor Radiometer on the Earth Observation System (AMSR-E): (a) 89 GHz h-pol, (b) 36.5 GHz h-pol.

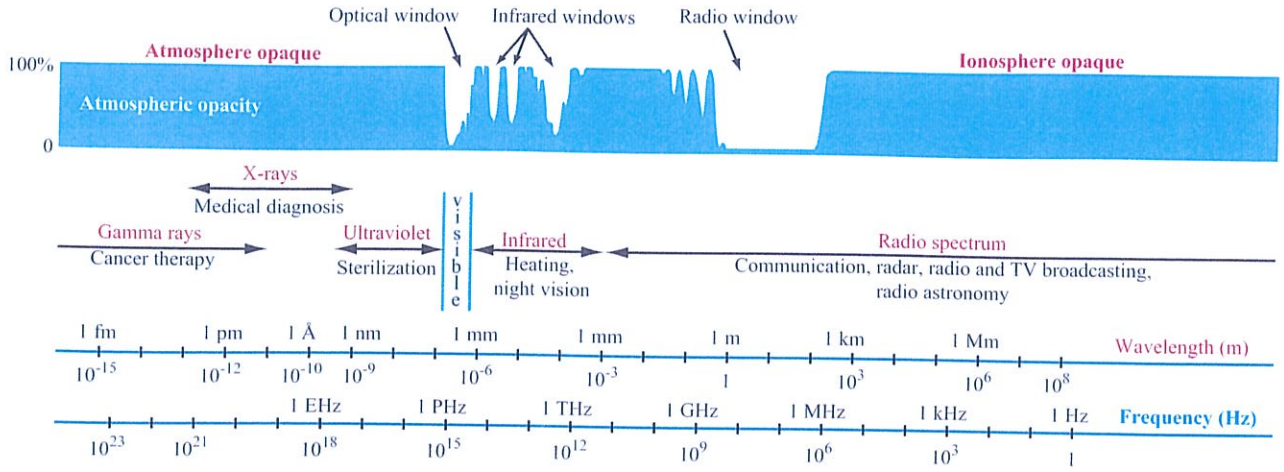

Figure 1-11: The electromagnetic spectrum. Atmospheric opacity for the Earth is shown along the top.

arms spanning 8 m, SMOS collected L-band radiometry measurements that could be processed to an effective spatial resolution of 35 km over a 1000 km wide swath (Kerr et al., 2010; Font et al., 2000).

1-4 The Electromagnetic Spectrum

Figure 1-11 provides a spectral plot of ***atmospheric opacity*** under clear-sky conditions. The electromagnetic spectrum spans over many decades in frequency (or wavelength). The lowest frequencies (longest wavelengths) constitute the radio spectrum, which includes the microwave portion of the spectrum. At higher frequencies (shorter wavelengths) above the radio-frequency spectrum lies the infrared spectrum, followed by the visible range. Above the visible spectrum lies the ultraviolet spectrum and, overlapping it, the X-ray spectrum. Finally, at the highest frequencies are the gamma rays. Remote sensing is practiced across most of the electromagnetic spectrum. However, our primary interest in this book is in the radio portion of the spectrum, and specifically in the microwave region. The atmospheric opacity, the ability of the signal to penetrate the atmosphere, is plotted along the top of Fig. 1-11. ***Atmospheric transmissivity*** (the inverse of

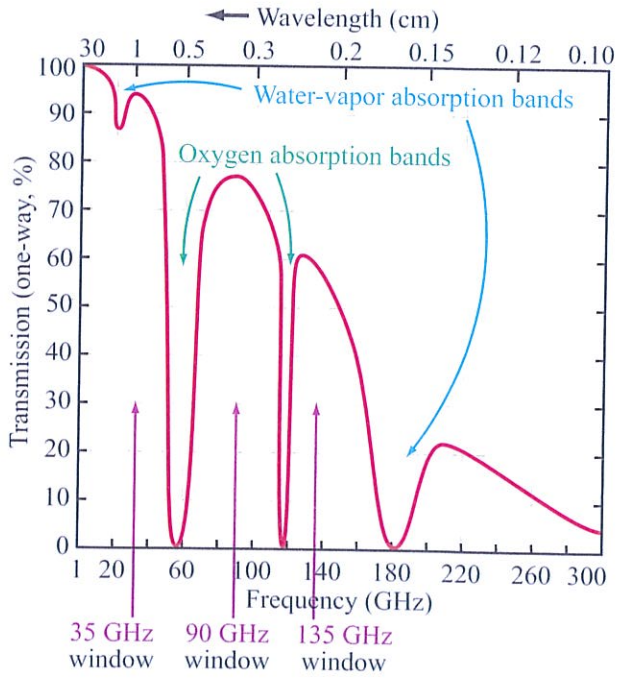

Figure 1-12: Percentage transmission through the Earth's atmosphere, along the vertical direction, under clear sky conditions.

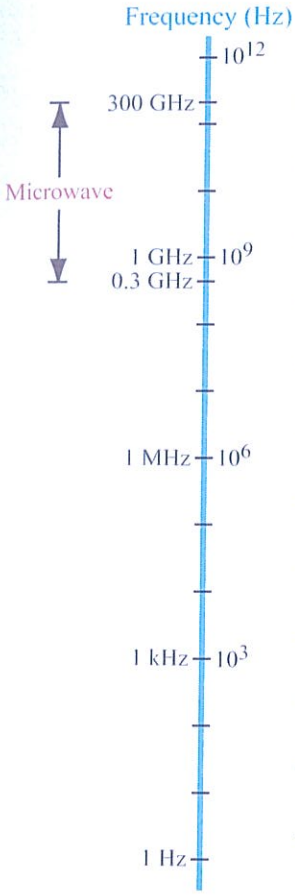

Band	Applications
Extremely High Frequency (30–300 GHz)	Radar, advanced communication systems, remote sensing, radio astronomy
Super High Frequency (3–30 GHz)	Radar, satellite communication systems, aircraft navigation, radio astronomy, remote sensing
Ultra High Frequency (300 MHz – 3 GHz)	TV broadcasting, radar, radio astronomy, microwave ovens, cellular telephone
Very High Frequency (30–300 MHz)	TV and FM broadcasting, mobile radio communication, air traffic control
High Frequency (3–30 MHz)	Shortwave broadcasting
Medium Frequency (300 kHz – 3 MHz)	AM broadcasting
Low Frequency (30–300 kHz)	Radio beacons, weather broadcast stations for air navigation
Very Low Frequency (3–30 kHz)	Navigation and position location
Ultra Low Frequency (300 Hz – 3 kHz)	Audio signals on telephone
Super Low Frequency (30–300 Hz)	Ionospheric sensing, electric power distribution, submarine communication
Extremely Low Frequency (3–0 Hz)	Detection of buried metal objects
	Magnetotelluric sensing of the Earth's structure

Figure 1-13: The RF spectrum and some of its applications.

opacity) over the microwave band is shown in Fig. 1-12. Atmospheric opacity and transmissivity play a key role in frequency selection for remote sensing within or through the atmosphere.

For example, because of water-vapor absorption near 22 and 183 GHz and oxygen absorption near 58 and 119 GHz, these frequencies are used almost exclusively for radiometric observations of the atmosphere. In contrast, because at frequencies below 20 GHz the atmosphere is essentially transparent, and in atmospheric "windows" signal attenuation is tolerable, sensors observing the Earth's surface through the atmosphere are operated at frequencies below 20 GHz and at those within the transmission windows shown in Fig. 1-12. Short-range radar applications such as vehicle anticollision radars operate at 77 GHz where atmospheric attenuation helps minimize interference from distant radars.

Figure 1-13 summarizes some of the applications of the radio spectrum, including communication, navigation, broadcasting, radar, and passive remote sensing. Since the spectrum is a finite resource, these services must share the spectrum, so national governments coordinate with international organizations such as the International Telecommunication Union (ITU) for this purpose. Letter designations adopted

Table 1-5: Common band designations (GHz).

Band	Frequency Range (GHz)
P	0.225–0.390
L	0.390–1.550
S	1.550–4.20
C	4.20–5.75
X	5.75–10.9
K	10.9–36.0
Q	36.0–46.0
V	46.0–56.0
W	56.0–100

internationally by the ITU are shown for decade regions of the spectrum.

► By convention, the *microwave region* encompasses the UHF, SHF, and EHF bands, extending from 0.3 to 300 GHz (1 m to 1 mm in wavelength). ◄

Numerous schemes of letter designation for bands within the microwave region exist. A commonly used set of these schemes is indicated in Table 1-5. The various bands also have official ITU subdesignations not identified here. Common usage, however, describes the lower part of *K-band* (by convention 10.9 to 22 GHz) as Ku-band, whereas frequencies above 22 GHz in the K-band are normally designated Ka-band. These designations are used commonly in spite of the existence of more precise definitions.

Radars may be found in all of the bands, with the possible exception of the Q- and V-bands, with most remote sensing radars operating at L-band or higher frequencies. Formal administrative approval (from the FCC in the U.S. or from agencies with a similar function in other countries; international frequency allocation is done at infrequent World Administrative Radio Conferences) in the form of a license is required for radar operation within specifically allocated frequency bands. Table 1-6 lists some of these allocations along with some selected non-remote-sensing allocations. Sharing between radar remote-sensing systems and

Table 1-6: Radar frequency allocations for remote sensing (GHz) summarized from the 1992 WARC. (All are shared with other services.)

1.215–1.300, 3.1–3.3, 5.25–5.35, 8.55–8.65
9.50–9.80, 13.4–14.0, 17.2–17.3, 24.05–24.25
35.5–35.6, 78.0–79.0

Examples of Other Allocations

Radar altimeter	4.2–4.4
Doppler navigator	8.8, 13.25–13.40
Meteorological radar	5.6–5.65, 9.3–9.5
Coastal radar	5.35–5.65, 9.0–9.2, 10.0–10.55
Ship radar	5.46–5.47, 9.3–9.5, 14–14.3, 24.25–25.25, 31.8–33.4

other radars is usually not permitted. Thus, the designer of a remote-sensing radar system cannot arbitrarily choose a frequency and use it.

Radiometers are also found throughout the microwave spectrum. The measurement precision of a microwave radiometer is proportional to $(B\tau)^{-1/2}$, where B is the receiver bandwidth and τ is the integration time. Since the radiometer is on a moving platform and may be scanning to achieve a wide swath, τ is typically constrained. Thus, to achieve precision radiometry it is desirable to use as wide a bandwidth as possible. However, since radiometers are very sensitive to interference, they usually use protected frequencies exclusively allocated for passive sensing. Allocations for these purposes are summarized in Table 1-7. Passive microwave systems share frequency allocations with radio astronomy, and these frequencies are protected against transmission of any kind. However, since some of the radio-astronomy bands are too narrow for airborne and spaceborne passive sensors, additional frequencies have been allocated for them on a shared basis (see Table 1-7), but users of such systems must be aware of the likelihood that some points on the globe will be inaccessible for their sensing because of interference from ground transmitters. No licenses are required for passive microwave remote sensing, though the designer must be prepared to deal with possible interference, even when operating within allocated passive-only bands. As an illustration, Fig. 1-14 shows a map of the

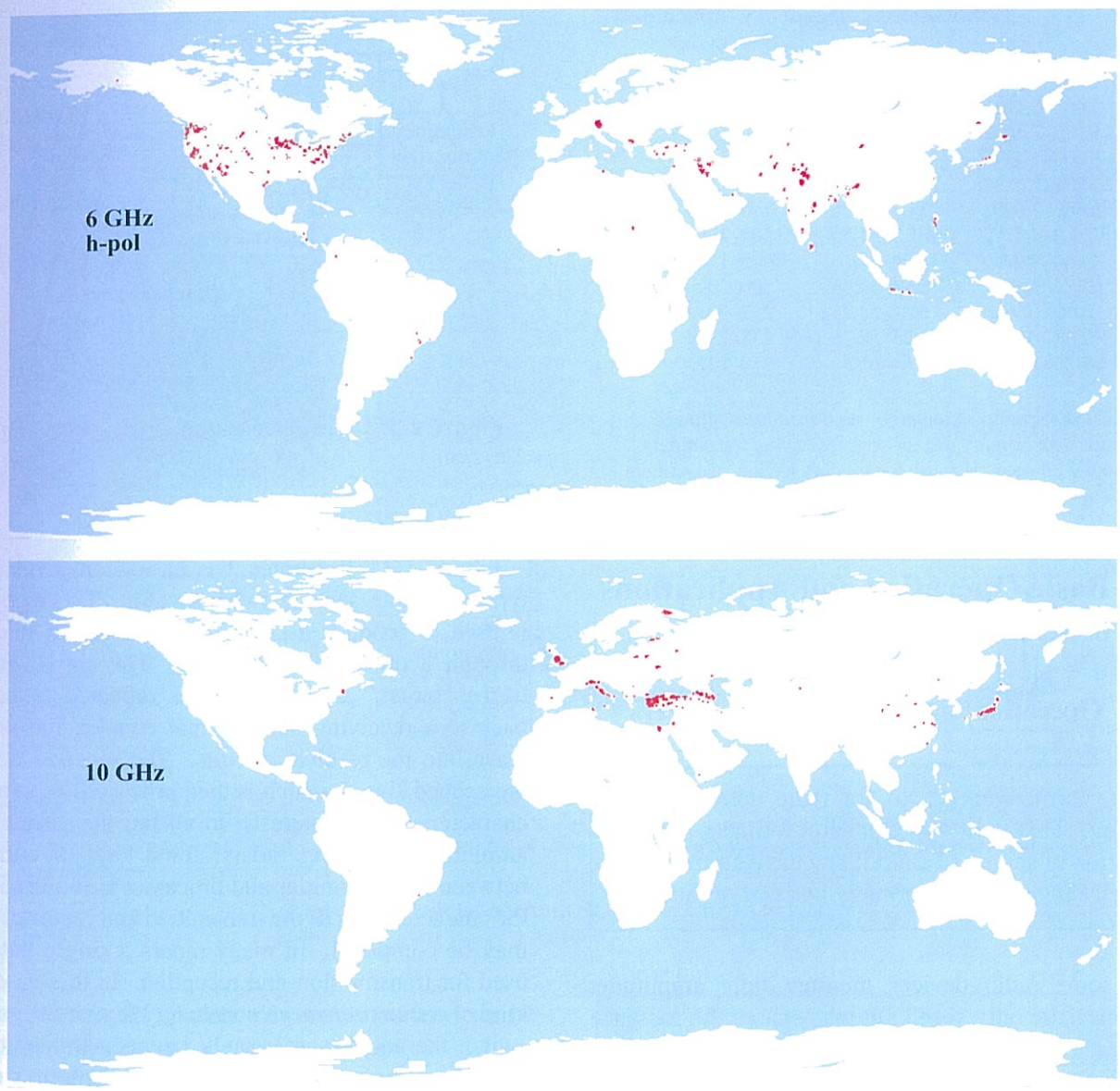

Figure 1-14: Intensity of radio frequency interference (RFI) observed by the WindSat polarimetric radiometer at 6 GHz h-pol and 10 GHz polarimetric. [Images courtesy of William Johnson and Li Li, Naval Research Laboratory.]

location of interference observed in 2008 by the WindSat polarimetric radiometer.

Table 1-7: Passive-sensor frequency allocations (GHz).

0.404–0.406a	15.35–15.40a	89–92a
1.370–1.400s	21.2–21.4p	100–102p
1.400–1.427s	22.21–22.5s	105–116a
1.6605–1.6684p	23.36–24.0a	116–126p
2.600–2.640s	31.3–31.5a	150–151p
4.2–4.4s	31.5–31.8p	164–168a
4.80–4.99s	36–37p	174.5–176.5p
6.425–7.250s	50.2–50.4p	200–202p
10.60–10.68p	51.4–54.25a	217–231a
10.68–10.70a	54.25–58.2p	235–238p
15.20–15.35s	64–65a	250–242a

a: protected for radio astronomy—no transmitters allowed;
p: shared, with primary use for services having transmitters;
s: shared, with secondary use for services having transmitters.

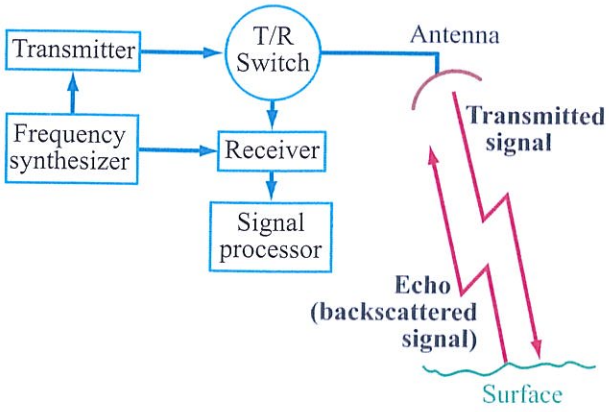

Figure 1-15: Basic elements of a remote-sensing radar system.

1-5 Basic Operation and Applications of Radar

1-5.1 Operation of Remote-Sensing Radars

► The term *radar* stands for radio detection and ranging. This term was coined at a time when the detection of ships and aircraft and the determination of their ranges was the primary purpose of radar. ◄

Today some radio devices measure only amplitude; others measure only speed. In many cases the presence of a target, such as the ground, is known; thus, "detection" may be unnecessary. The term "radar" is now applied to any radio device in which a transmitter illuminates a reflecting or scattering surface or object and a receiver measures some property of the reflected signal. Fundamentally, a radar can determine (1) direction (by the pointing of the antenna), (2) distance (by measuring the time of flight of the signal to and from the target), (3) speed (by measuring the Doppler shift of the echo), and (4) radar scattering cross section (by comparison of the energy of the echo return to that of the transmitted signal).

Figure 1-15 illustrates the basic components of a typical remote sensing radar system. The ***transmitter*** is used to produce a signal that is coupled into space through a transmitting antenna. The signal goes out to the "target," from which it is reflected or scattered back to a receiving antenna that couples the scattered wave into the receiver circuits. The ***receiver*** amplifies the echoed signal, which is then processed to extract the characteristics of interest. In all but the very simplest amplitude-measuring radars, some kind of correlation between the transmitter and processor is required so that the characteristics of the transmitted and received signals may be compared. In many radars a single antenna is used for transmission and reception. In this case, some kind of a ***transmit-receive switch*** (TR switch) is used to switch the antenna alternately between transmitter and receiver, although with some radars, isolation may be achieved by the use of a ***microwave circulator***. Radar system design and operation is described in more detail in Chapters 13–16.

As previously noted, radar systems used for remote sensing fall into broad categories: ***imaging radars*** (SAR and SLAR), and nonimaging radars such scatterometers, altimeters, and meteorological radars. Many remote-sensing applications call for an imaging radar, but specialized applications, such as measuring winds at sea, use scatterometers. Though classified as a

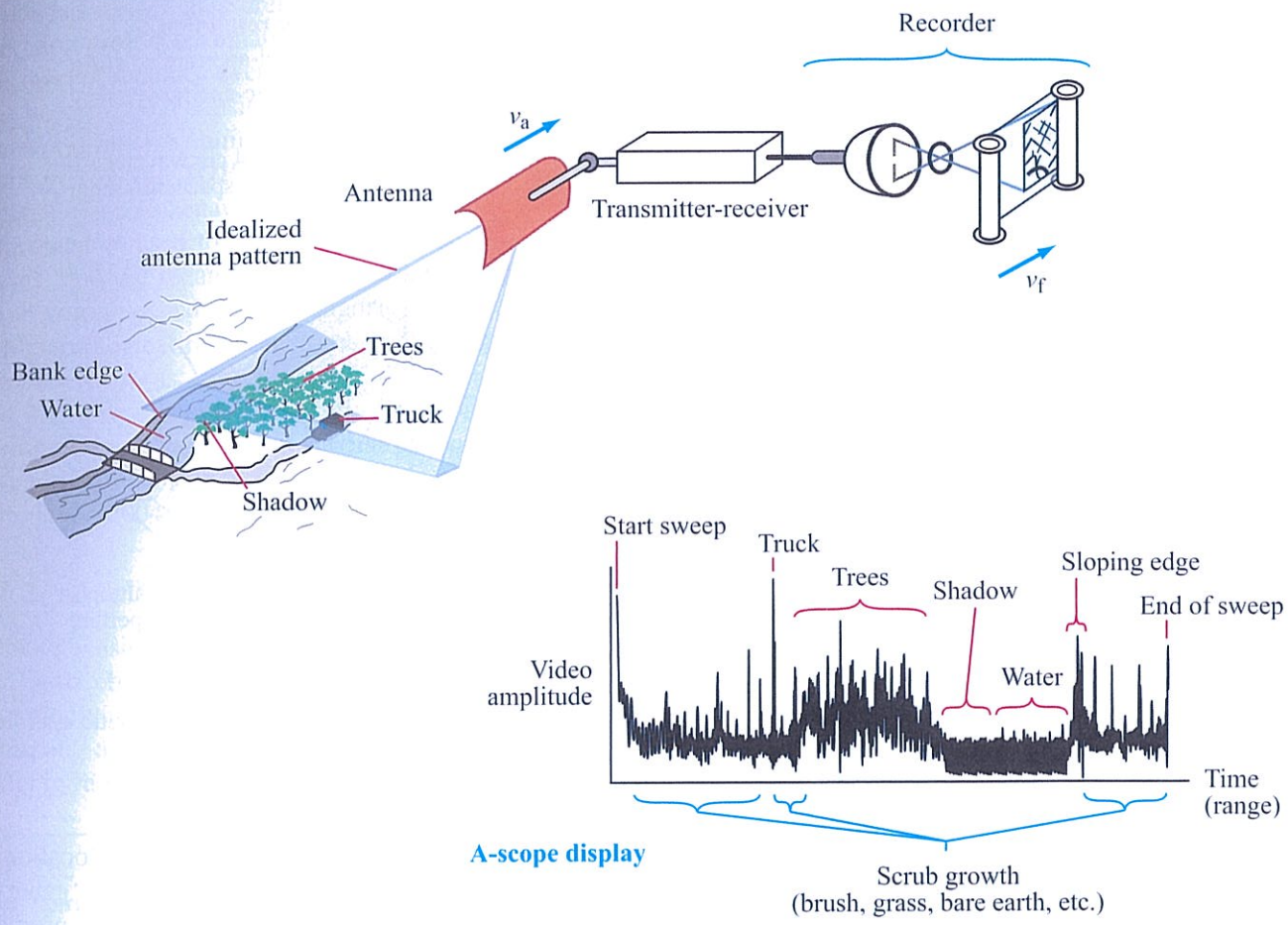

Figure 1-16: Real-aperture SLAR imaging technique.

nonimaging sensor, spaceborne scatterometers can be used to generate low-resolution imagery.

In side-looking airborne radar (SLAR) imaging, the antenna points to the side with a beam that is wide vertically and narrow horizontally. The image is produced by motion of the aircraft past the area being covered, as illustrated in Fig. 1-16. In this simple pulsed system, a short pulse is transmitted from the airborne radar, primarily within the horizontally narrow beam shown. When the pulse strikes a target, a signal returns to the aircraft.

► The time delay associated with this received signal, as with other pulse radars, gives the distance between target and radar. ◄

The picture illustrates a typical return at a particular instant in the flight, with strong signals coming from clumps of trees and bridges and no signal coming from the radar "shadow" of a stream bed. When a single pulse is transmitted, the return signal can be displayed on an oscilloscope as shown in Fig. 1-16. In early SLAR systems, the intensity of the signal was recorded on a moving strip of film that moved synchronously

with the motion of the aircraft, so that as the aircraft moved forward the film also moved. As the aircraft moved, the series of intensity lines formed an image, a two-dimensional picture of the radar-return from the surface. In practice, film-based recording has significant limitations and modern systems store the data digitally.

► Side-looking airborne radars can be divided into two groups: real-aperture systems that depend on the beamwidth determined by the actual antenna, and synthetic-aperture systems that depend upon platform motion and signal processing to achieve a much narrower beamwidth in the along-track direction than that attainable with the real antenna alone. ◄

The customary nomenclature used is "SLAR" for the real-aperture system and "SAR" for the synthetic-aperture radar (SAR) system, although the latter is also a type of a side-looking airborne radar.

The along-track resolution of a SLAR is proportional to the product of the antenna beamwidth and the distance to the target. Thus, the resolution of a SLAR varies with cross-track distance and large antennas are required for fine resolution. A major advantage of SAR over SLAR is that the resolution of the SAR in the along-track direction is proportional to the length of the synthetic antenna and is independent of the distance. (This key result is derived in Chapter 14.) Thus, a SAR may be used in either an aircraft or a spacecraft without compromising the along-track resolution. Unlike SLAR, fine resolution for a SAR requires a *short* antenna rather than a long one! Figure 1-17 illustrates how SAR combines data collected from multiple antenna positions to synthesize a longer effective antenna, thereby achieving high along-track resolution. Many modern SAR systems include multiple polarization or polarimetric capabilities that yield information on scattering mechanisms and enhance the utility of the SAR image data (Ulaby and Elachi, 1990; Cloude and Pottier, 1996; Touzi et al., 2004).

The most commonly used nonimaging remote-sensing radars include meteorological radars, scatterometers, and altimeters. ***Wind scatterometers*** collect

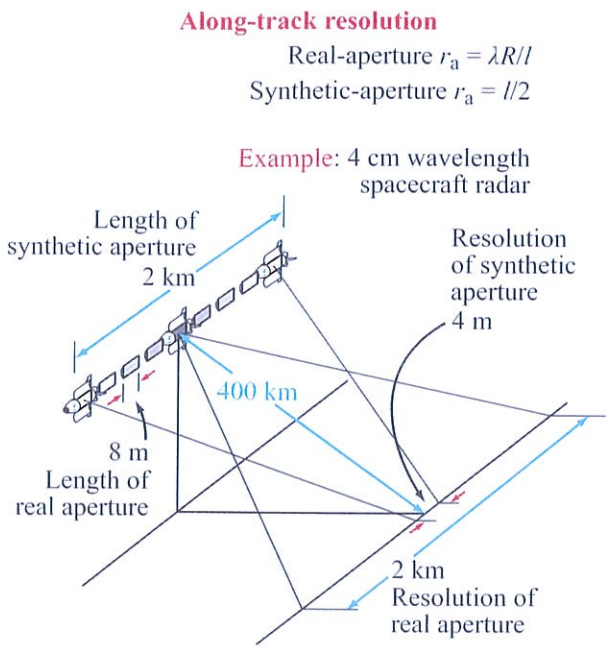

Figure 1-17: An illustration of how synthetic aperture works.

backscatter measurements of the same location at multiple aspect angles and/or frequencies, generally over a wide swath. Accurate backscatter measurements are the essential function of a scatterometer. Careful attention to thermal design and internal calibration schemes are required to achieve the desired accuracy over a time period of up to a decade for spaceborne systems. For ocean measurement they must make multiple measurements over a diversity of incidence and/or azimuth angles. This is accomplished with either multiple fan-beams (Naderi et al., 1991) or with rotating pencil-beam antennas (Spencer et al., 1997), as illustrated in Fig. 1-7. For fan-beam antennas, Doppler processing and/or range gating is used to obtain along-beam resolution.

► Satellite altimeters measure the distance between the platform and the surface with a measurement accuracy on the order of 1 cm. ◄

While radar range measurement accuracy is critical, high precision orbit determination is also required to achieve this level of accuracy over the ocean (Zieger et al., 1991). The need to avoid aliasing from tides leads to the use of unusual orbits for altimeters, such as the 1600 km orbit employed by the *TOPEX/Poseidon* mission (Fu et al., 1994; Fu and Cazenave, 2001). The shape of the pulse return can be used to extract information about surface waves, and the mean backscatter provides information about wind-induced surface roughness.

Meteorological radars measure radar backscatter and *Doppler shift* as a function of distance to observe and map precipitation and wind. They often combine multiple beams in rotating antennas along with range gating to collect data in three dimensions (Cobb, 2004; Meischner, 2004).

1-5.2 Applications of Remote-Sensing Radars

Remote-sensing radar has become a standard tool for Earth observation and new applications are being continually developed. Table 1-8 summarizes some common applications of airborne and spaceborne imaging radars (SLAR and SAR) in remote sensing.

► The primary application of nonimaging radars to remote sensing is in oceanography and polar ice, where spaceborne radar altimeters and scatterometers are used. ◄

The altimeter has been used to measure the detailed characteristics of the geoid, to establish characteristics of tides and even of current flows by very precise measurement of the deflection of the ocean associated with the currents (Fu and Cazenave, 2001; Leitao et al., 1978), and to determine the height of waves directly beneath the spacecraft (Gower, 1979). Such information aids in predicting El Niño and La Niña events. Radar scatterometers enable accurate determination of the wind speed and direction over the ocean, as well as rain rate (Naderi et al., 1991). Scatterometers have also been used for sea-ice mapping and iceberg tracking as well as soil moisture and vegetation. Reconstruction-based processing techniques (Early and Long, 2001) have been developed to enable scatterometers to be used as imaging sensors, which has helped expand their applications.

Radar imaging has been used extensively in support of many geologic applications. It is used in identifying

Table 1-8: Selected applications of airborne/spaceborne imaging radar in remote sensing.

Geology:
Structure
Lithology
Hydrology:
Soil moisture
Watershed mapping
Flood mapping
Mapping of surface water (ponds, lakes, rivers)
Snow mapping
Agriculture:
Crop mapping
Agricultural-practice monitoring
Identifying field boundaries
Monitoring growth and harvest progress
Identifying stress areas
Rangeland monitoring
Water problems–same as hydrology
Forests:
Monitoring cutting
Mapping fire damage
Identifying stress areas
Vegetation density
Cartography:
Topographic mapping
Land-use mapping
Monitoring land-use changes, urban development, etc.
Polar regions (cryosphere):
Monitoring and mapping sea ice
Detecting and tracking icebergs
Mapping glacial ice sheets
Monitoring glacial changes, including measuring velocity
Ocean:
Measuring wave spectra
Monitoring oil spills
Monitoring ship traffic and fishing fleets
Wind speed and direction measurement
Rain
Clouds
Measuring currents
Undersea mapping

geologic structures with the goal of mineral exploration and general geologic mapping; of lesser importance is the direct determination of lithologies. This is effective in desert regions where the rocks are exposed, but less so in heavily vegetated regions where the radar signal comes largely from the vegetation, since differences in the underlying rock cannot be detected except by surrogates in the vegetation signature.

While scatterometers have been used for soil moisture mapping, imaging radar has not yet been used operationally for soil moisture determination, though experiments have demonstrated that SAR images do provide useful soil moisture information (Ulaby et al., 1974, 1979, 1982a; Oh et al., 1992; Dubois et al., 1995a). Radar images have been used for mapping floods, a task made easy by the strong contrast between a body of water and a land surface. Missions such as SMAP are planned to provide global soil moisture mapping from space (Entekhabi et al., 2010). This mission will also enable mapping the extent, water content, and state of snow cover, which are important in determining future runoff and whether to forecast floods or the amount of water that will be available for irrigation or hydroelectric power generation (Stiles and Ulaby, 1980a).

Radar is particularly useful in polar regions because of the long period of darkness and the extensive presence of ice fogs, both of which limit the use of sensors at visible wavelengths. Radar's ability to map the characteristics of sea ice has been well demonstrated (Page and Ramseier, 1975).

Spaceborne SARs have been used for lake and ice monitoring and have been used extensively to map glacial ice and determine the speed of glacier flow in Greenland, Antarctica, and other regions (Jezek, 2003). SAR images are used operationally to map sea ice and to detect and track icebergs in the polar regions. Computer-based techniques for spatially combining and processing scatterometer measurements have made it possible to produce scatterometer (and radiometer) imagery suitable for many applications. While scatterometer images are of much lower resolution than the images generated by SLARs and SARs, they are finding important applications in climate research, particularly in the polar regions.

The Seasat SAR first demonstrated that certain characteristics of wave patterns can be monitored on a global scale (Beal, 1980). Since then, most spaceborne SARs now include a "wave mode" to measure the ocean surface wave spectrum and detect and track oil spills (Kraus et al., 1977; Moncrief, 1980; Lehner et al., 2000). Because the radar signal from the ocean's surface is largely determined by capillary waves, which are dampened by the presence of oil, a dark area in an ocean image can be an indication of an oil layer. Though of lower resolution, scatterometer images can also be used for mapping large oil spills (Lindsley and Long, 2012). The ability of radar to monitor ship traffic, both from the shore and from other ships, is well known and is being exploited by spaceborne SARs such as ***TerraSAR-X*** (Moreira and Bamler, 2010).

1-6 Basic Operation and Applications of Radiometers

1-6.1 Radiometer Operation

Unlike the signal received by a radar, which consists of energy scattered back by the target after it has been illuminated by the radar's transmitting antenna, the "transmission source" for a radiometer is the target itself, and the radiometer is merely a passive receiver. The energy received by a radiometer is due to radiation emitted and/or reflected by the scene and collected by the antenna. The total-power radiometer shown in Fig. 1-18 consists of an antenna, an amplifying predetection section, a detector, an integrator (low-pass filter) and a recording device.

As discussed in detail in Chapter 6, the power P emitted by an object in thermodynamic equilibrium is a function of its physical temperature T, and in the microwave region P is directly proportional to the ***brightness temperature*** T_B,

$$P = kT_B B, \tag{1.1}$$

where k is Boltzmann's constant and B is the radiometer bandwidth. If the material has a constant physical

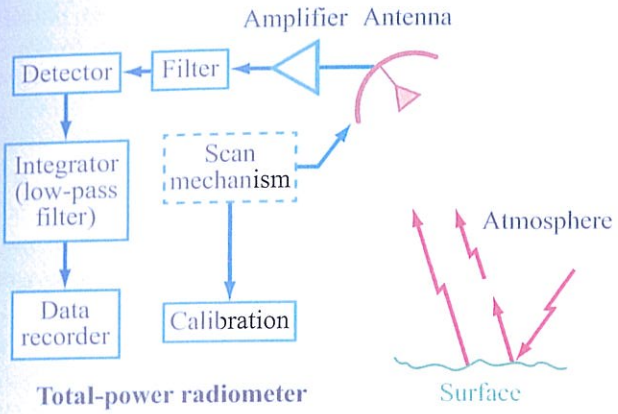

Figure 1-18: Key elements of a microwave radiometer.

temperature T, the material is said to have an emissivity $e = T_B/T$ where e varies between 0 for a perfectly nonemitting material and 1 for a perfect emitter known as a *blackbody*.

Ideally, if the scene observed by the antenna beam is characterized by a uniform brightness temperature T_B (representing radiation in the direction of the antenna), then the observed antenna power is the same as P. In reality, however, the observed power represents all radiation incident upon the antenna, integrated over all possible directions and weighted according to the antenna directional pattern. Other factors play an important role, including the effects of the atmosphere and self-emission by the antenna structure, as well as noise generated internal to the receiver. These factors are considered in Chapters 6 and 7.

While it was stated earlier that a radiometer is merely a passive receiver, a radiometer receiver differs from a traditional radar or communications receiver in two key respects. First, whereas the input signal that is processed by a traditional receiver may be phase-coherent and nearly monochromatic, the natural radiation emitted by material media is phase-incoherent and extends over the entire electromagnetic spectrum. That is, it is "noiselike" in character and similar to the noise power generated by the receiver components.

The second difference relates to the *signal-to-noise* ratio, S_n, at the receiver output. In traditional receivers, faithful extraction of the information contained in the received signal necessitates that $S_n \gg 1$ to differentiate the signal from the fluctuating component of the noise. This condition usually is achieved through a combination of amplitude and waveform design of the transmitted signal and the application of signal-processing techniques in the receiver section, although scatterometers often use methods similar to those used in radiometers (Chapter 7). However for radiometers, the radiometric signal to be measured usually is much smaller than the receiver noise power. Highly sensitive receivers with processing that averages in time and frequency are required to extract precise measurements of T_B. High stability and precise, frequent calibration are also required. To aid in this, several different receiver configurations have been developed, some of which are discussed in Chapter 7.

Typical radiometers measure T_B of both vertically polarized and horizontally polarized signals, each of which conveys information about the scene. As explained later in Chapter 7, in *polarimetric radiometry* all four Stokes polarization parameters are measured (Gasiewski and Kunkee, 1993; Tinbergen, 1996) from which more information about the observed scene can be inferred.

1-6.2 Applications of Microwave Radiometry

▶ Microwave radiometry is used for (1) astronomical studies, (2) military applications and (3) environmental monitoring. ◀

Although both radars and radiometers are employed in radio astronomy, Earth-based radars are limited to observations of the sun and nearby targets such as the planets and moons within the solar system. Radiometers, on the other hand, have been used to measure the radio emission from numerous objects in our galaxy, as well as from objects in other galaxies.

The primary military use of radiometers has been for detecting or locating metal objects. As was mentioned earlier, the term used for characterizing the emission by the scene observed by the radiometer (through its

antenna beam) is the brightness temperature T_B, which may vary from zero kelvins (for a nonemitting medium) to a maximum value equal to the physical temperature T_0 of the scene (for a perfect emitter known as a blackbody). Equivalently, the emissivity e $(= T_B/T_0)$ varies between zero and unity. Theoretically, a perfectly conducting material, such as a metal object, has zero emissivity, thereby making it easy to differentiate from the Earth's background (the emissivity for land surfaces is rarely < 0.3 and is often > 0.7). Although metal objects do not self-emit, their radiometric temperatures are not identically zero because they reflect downward-emitted sky radiation. The radiometric contrast between a ***field of view*** (FOV) with and without a metal target contained in it is a function of the ***beam-fill factor*** (ratio of the cross-sectional area of the metal target to the area of the antenna footprint on the ground). The size of the footprint (i.e., the spatial resolution) is governed by the distance between the radiometer and the ground and by the antenna beamwidths, the latter being in turn determined by the size of the antenna and the microwave frequency. Because of its inherently limited spatial resolution even at high microwave frequencies, a missile-borne microwave radiometer used for locating military targets can detect successfully the presence of the target only if the target is within a few hundred meters. A study conducted by Deitz and Constantine (1979), for example, shows that a 35 GHz radiometer at an altitude of up to 100 m above the ground can easily detect a tank against the signal fluctuation due to the ground surrounding it. This altitude range may be increased by a factor of 3 to 4 by operating at higher microwave frequencies, such as the atmospheric-window frequencies located at 94 and 140 GHz, because, for a given antenna size, the FOV varies as the square of the height-to-frequency ratio, $(h/f)^2$. Operationally, microwave radiometers are used in conjunction with other superior spatial-resolution sensors such as radars and infrared scanners, which serve as the prime sensors for detecting the presence of military targets. Microwave radiometers are used as the prime sensors in the final stage as a missile approaches a target area, since no warning signal is emitted by a radiometer. Because the microwave radiometer is a wideband incoherent receiver, its output fluctuates less as the antenna beam scans over a relatively homogeneous terrain than does the output from a "coherent" radar system. This smaller fluctuation translates into a lower probability of false alarm for the radiometer if the target's brightness temperature T_B is different from that of the background.

In addition to their use in radio astronomy and for military applications, microwave radiometers have found extensive use in several geoscientific fields, including meteorology, oceanography, and hydrology (see Table 1-9). The coarse spatial resolution of satellite microwave radiometers that have flown on satellites to date (see Table 1-4) limits their use to applications

Table 1-9: Selected applications of airborne/spaceborne microwave radiometers in remote sensing.

Hydrology:
- Soil moisture
- Watershed surface drainage
- Flood mapping
- Mapping of surface water (ponds, lakes, rivers)
- Snowcover extent, snow water equivalent, snow wetness

Agriculture:
- Soil moisture distribution for crop yield estimation and irrigation scheduling
- Delineation of freeze-thaw boundaries

Polar regions (cryosphere):
- Monitoring and mapping sea ice and sea-ice type
- Mapping glacial ice sheets
- Monitoring ice-sheet melt conditions

Ocean:
- Measuring surface wind speed
- Measuring surface temperature
- Measuring surface salinity
- Monitoring oil spills
- Measuring and mapping rain

Meteorology and climatology (primarily over the ocean):
- Temperature profile
- Integrated water vapor
- Water vapor profile
- Liquid water (rain)

Stratosphere, mesosphere, and lower thermosphere:
- Atmospheric temperature profile
- Magnetic field profile
- Abundance of atmospheric gases

compatible with resolutions of the order of 15 km or larger. This means that, with the exception of a few land applications, most radiometric applications are associated with observations of oceanographic parameters or atmospheric parameters over the ocean. These parameters include sea surface temperature and wind speed (Wilheit, 1979), sea-ice type and concentration (Zwally and Gloersen, 1977), atmospheric water-vapor content, liquid-water content, and temperature profiles (Staelin et al., 1973; Wilheit, 1979), rainfall rates (Wilheit et al., 1977), and salinity (Pampaloni and Paloscia, 2000), among others (Narvekar et al., 2007).

Over land, radiometers have proven useful in soil-moisture determination (Newton and Rouse, 1980) and snow accumulation (Chang et al., 1982). These applications are sensitive to soil-surface roughness and (to a lesser extent) vegetation cover. For this reason soil-moisture systems use lower frequencies, which are less sensitive to these confounding parameters. The SMAP mission will include an active sensor operating at essentially the same frequency as the radiometer in order to estimate and thus remove the vegetation contribution (Entekhabi et al., 2010).

Ocean wind speed and direction measurement are currently the primary application of polarimetric radiometry. The wave structure leads to azimuthal variations in the Stokes brightness temperature from which the vector wind creating the wave structure can be estimated using measurements from only a single azimuth direction (Yueh et al., 1994, 1995; Gaiser et al., 2004).

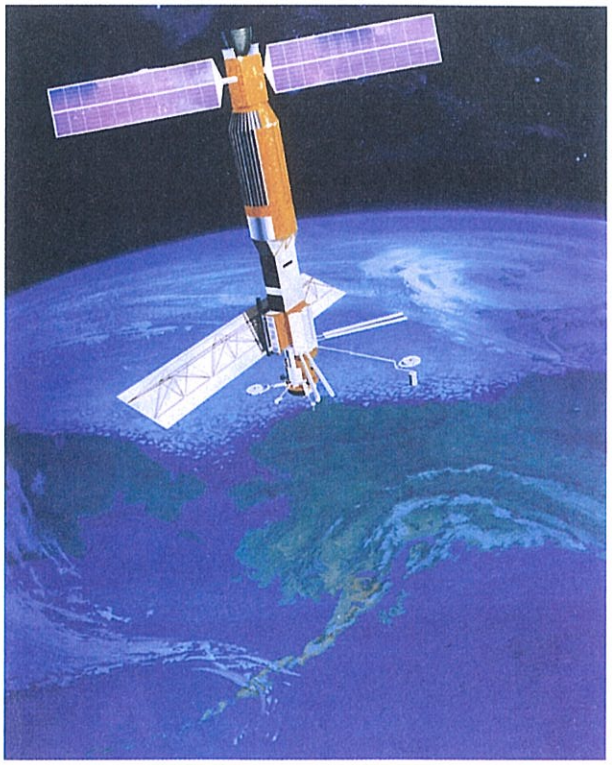

In 1978, the Seasat satellite carried the first civilian SAR in space.

1-7 Image Examples

To introduce the reader to the types of products generated by active and passive microwave sensors, we present Figs. 1-19 through 1-24. These are typical image products that display either the signal backscattered or emitted by a scene, or geophysical quantities derived from them. These six illustrative examples, along with Figs. 1-8, 1-9, and 1-10, are merely the tip of the iceberg, with many more included in later chapters. High-resolution versions of these images are available on the book's website (www.mrs.eecs.umich.edu).

Figure 1-19: This figure presents a Ku-band SAR image collected over Washington, D.C. The SAR illumination is from the top. Man-made features, such as buildings and bridges, stand out clearly in this radar backscatter image. The backscatter intensity of water is much smaller than that of buildings and vegetation, so water shows up black in the image. Individual trees can be distinguished in some areas, and the pattern of roads and urban development is clearly apparent. The Capitol building is left of center with the Mall extending to the right. Right of center is the Washington Monument, though only the shadow of the obelisk is readily apparent in the image. Just below the monument are the Ellipse and the White House. The Naval Research Laboratory is at the upper left. [Courtesy of Sandia National Laboratory.]

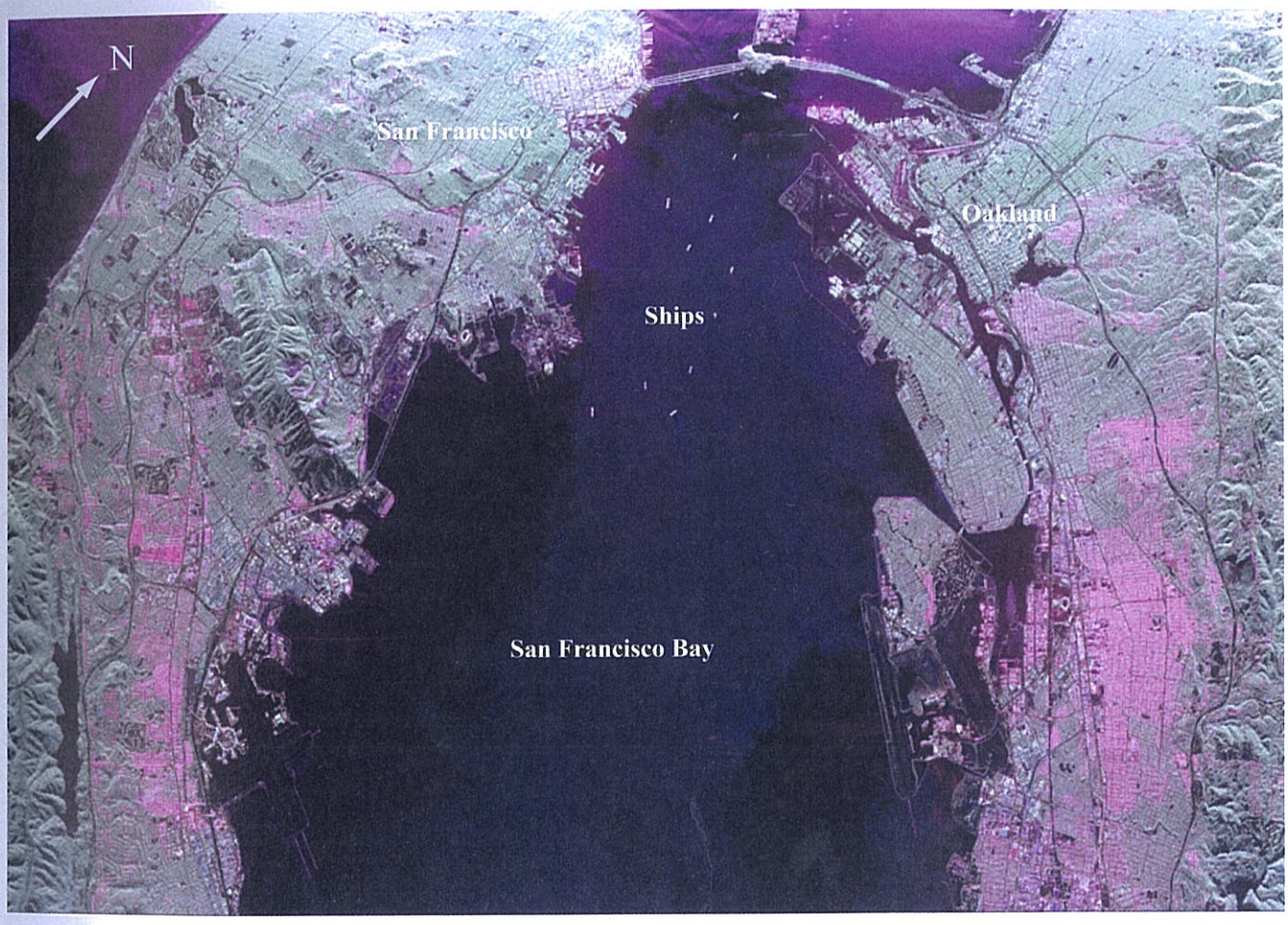

Figure 1-20: SAR image of a portion the San Francisco Bay area. Color describes the polarimetric backscatter for each pixel. The orientation of streets and roads in urban areas alters the polarimetric response in these areas, so the color is related to road orientation relative to the radar view direction, which is from the top. Water has low backscatter and appears dark. The Pacific Ocean is the dark area at the left, while San Francisco Bay is in the center. Bright objects in the bay are ships. The city of San Francisco, at the upper left, is connected to Oakland via the San Francisco-Oakland Bay Bridge, which passes through Yerba Buena Island at the top center. San Bruno Mountain is visible left of center and south of San Francisco. San Andreas Lake lies along the San Andreas fault at the western edge of the mountains at the lower left. [Courtesy of the Jet Propulsion Laboratory.]

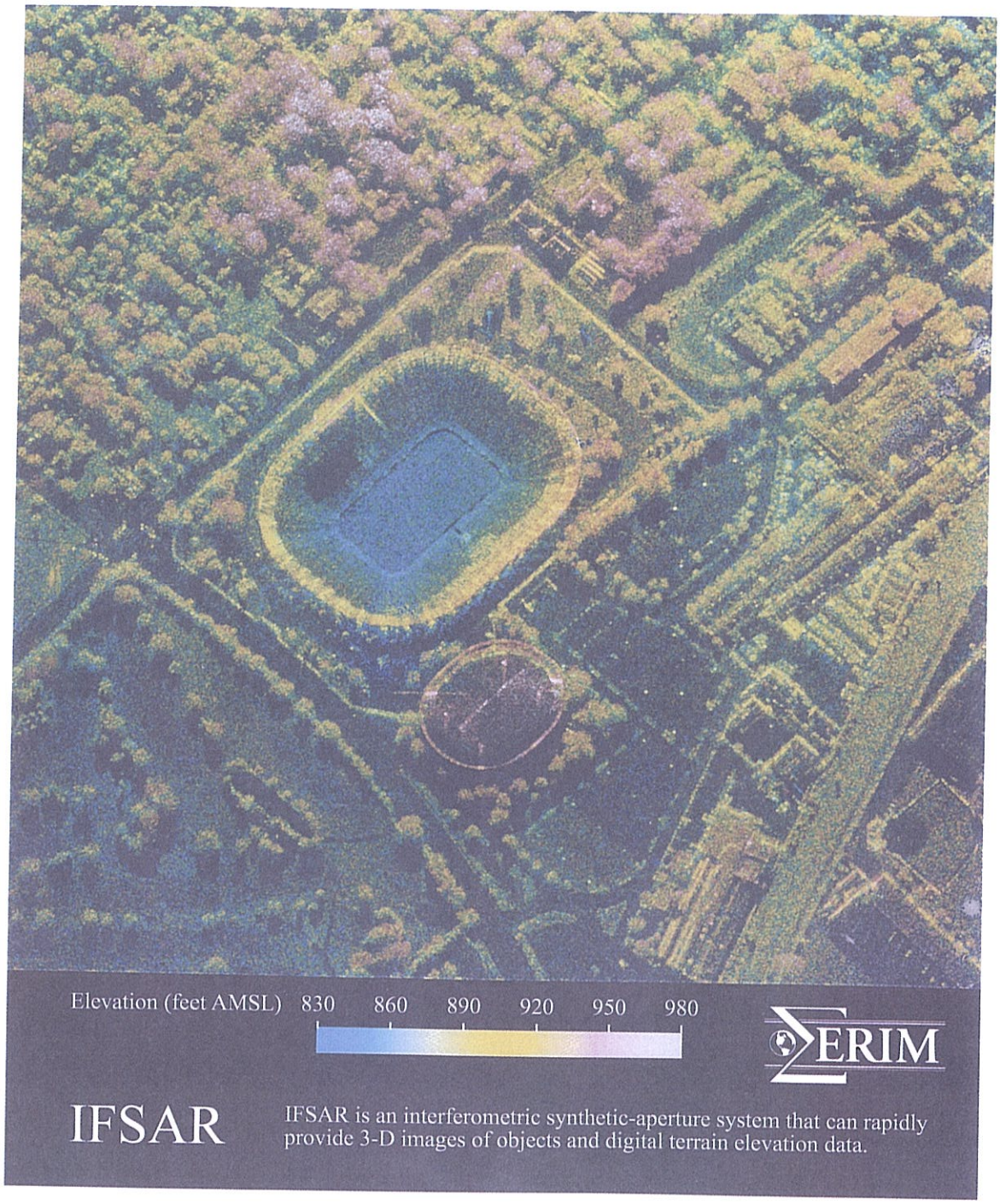

Figure 1-21: This SAR image is overlaid on a height map (color) derived using an interferometric SAR (IFSAR) technique. The image is one of the earliest demonstrations of SAR interferometry. Radar illumination is from the top. The University of Michigan football stadium is visible in the image center. Note that the playing field is depressed relative to the stands. The heights of individual trees growing on the rise in the image center can be seen. [Courtesy of the Environmental Research Institute of Michigan.]

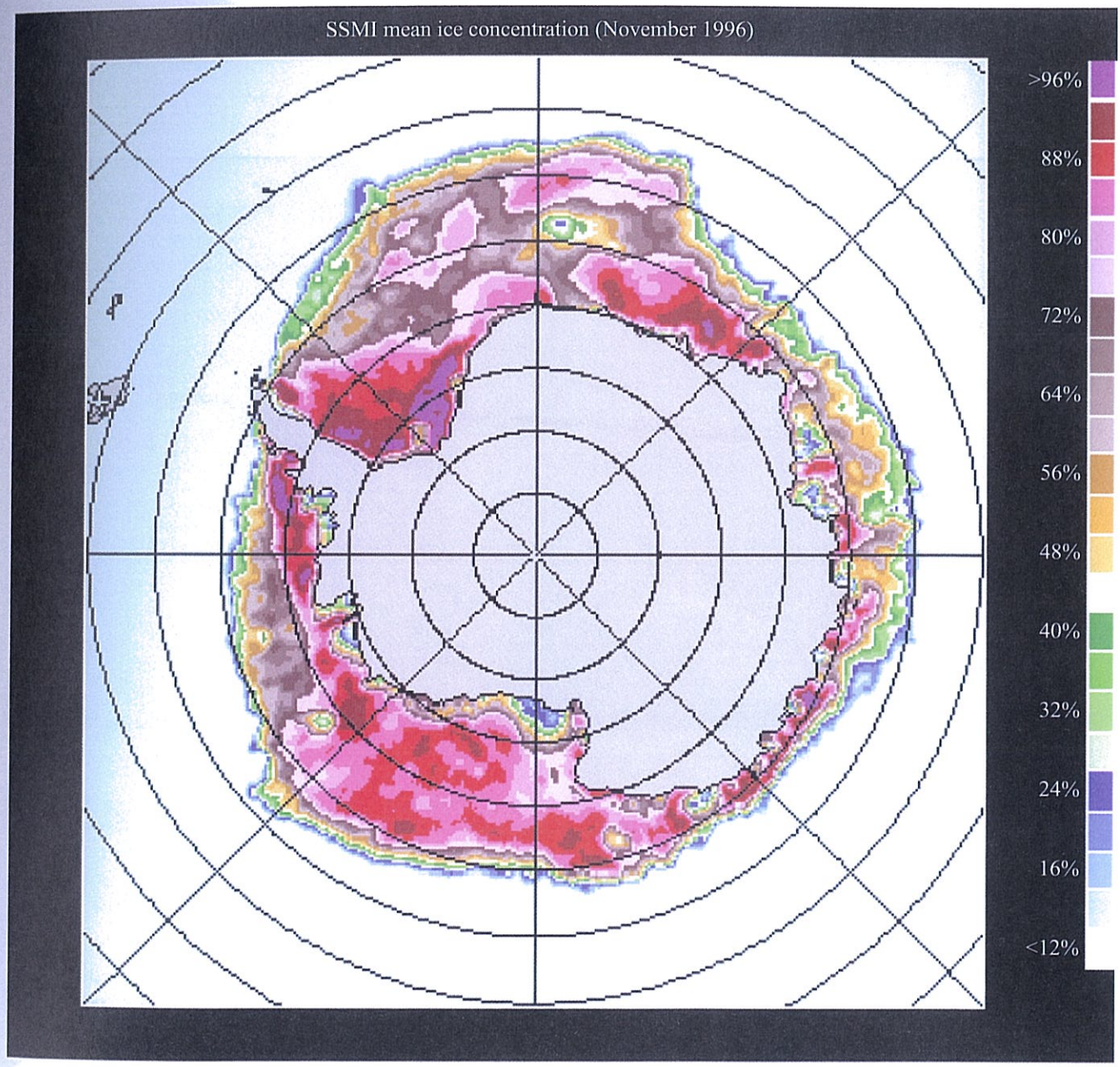

Figure 1-22: This map of sea-ice concentration in Antarctica is based on passive multichannel microwave measurements. For each pixel, the pixel color denotes the fractional amount of the pixel area covered by sea ice, with the remaining area of the pixel being open ocean. Land and near-land areas are masked off. Sea-ice coverage is an important factor in Earth's climate heat balance. [Courtesy U.S. National Sea Ice Data Center.]

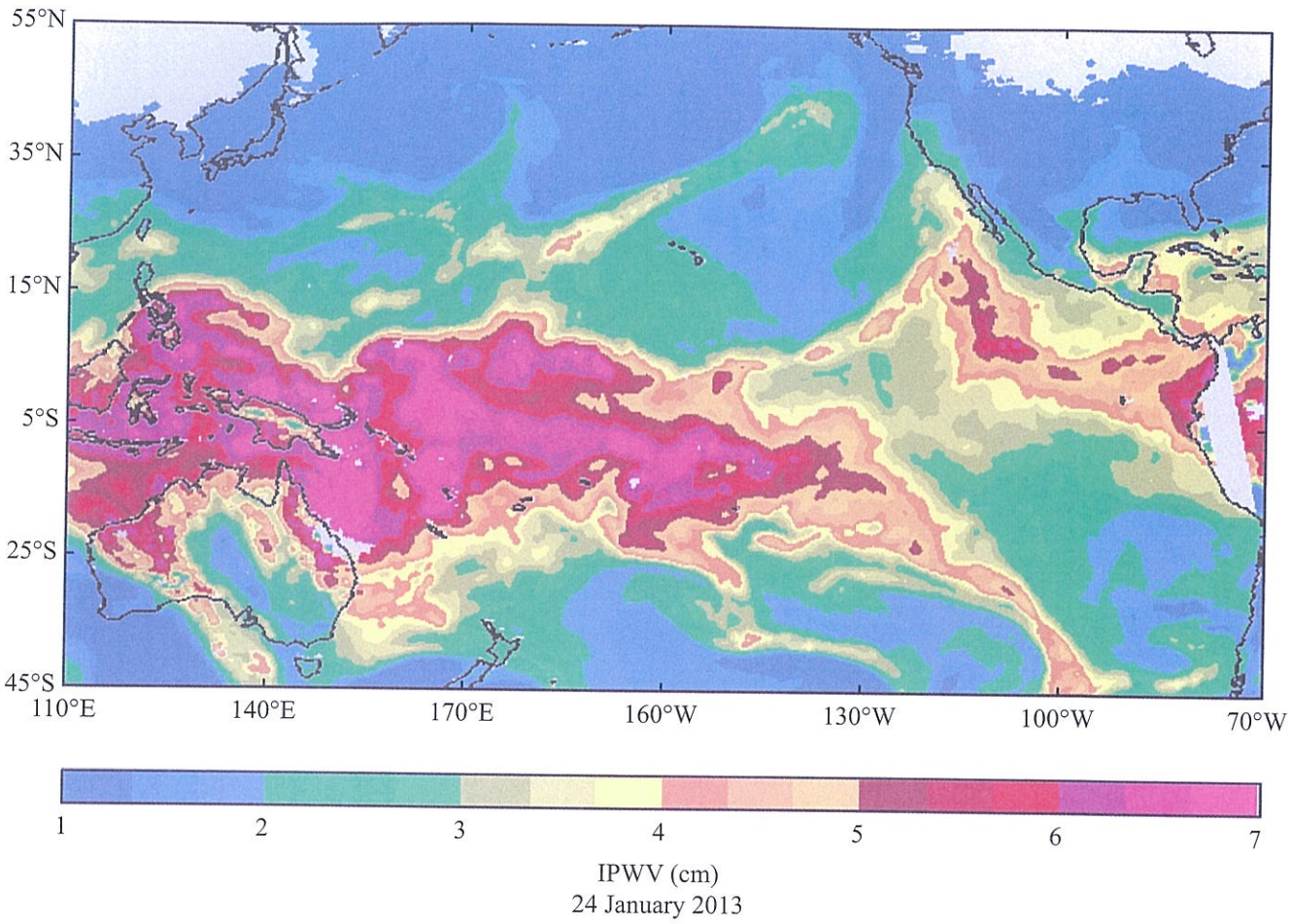

Figure 1-23: A map of integrated precipitable water vapor (IPWV). This is an important parameter used for predicting heavy precipitation. It also affects the heat balance of the atmosphere and is thus critical in climate modeling. This 6-hour-average map is derived from passive multichannel microwave observations from multiple satellite platforms and sensors whose measurements have been histogram matched (Kidder and Jones, 2007). The high values of IPWV along the southern tropical convergence zone south of the equator are indicative of high evaporation and convective rain. IPWV is measured in centimeters of equivalent precipitable water. [Courtesy of National Oceanic and Atmospheric Administration.]

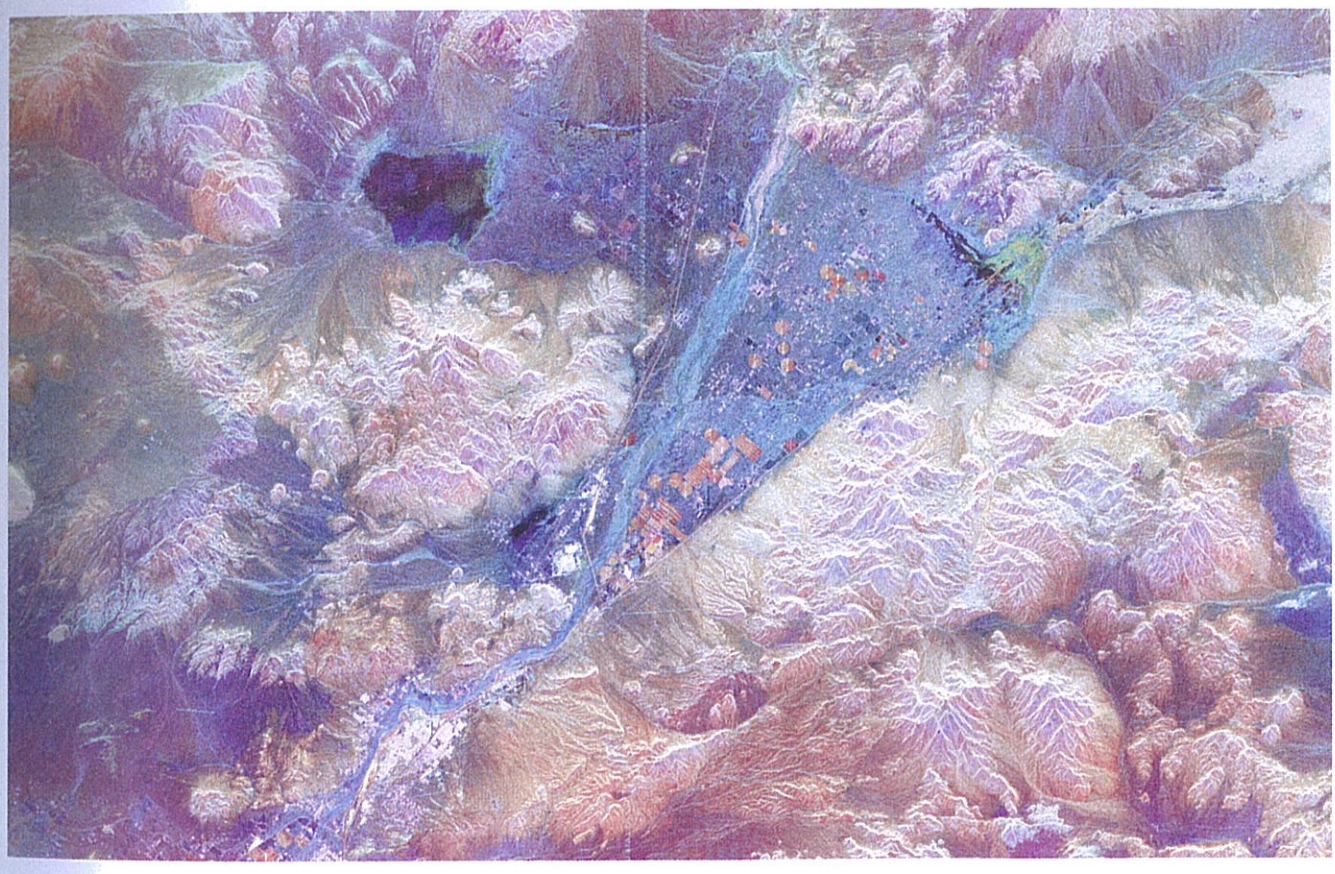

Figure 1-24: This spaceborne radar image shows part of the Mojave Desert in the vicinity of Barstow, California. [Courtesy of NASA/JPL.]